

QR-LoRA: Efficient and Disentangled Fine-tuning via QR Decomposition for Customized Generation

Jiahui Yang^{1,2} Yongjia Ma² Donglin Di² Hao Li² Wei Chen² Yan Xie²

Jianxun Cui^{*1} Xun Yang³ Wangmeng Zuo¹

¹ Harbin Institute of Technology ² Li Auto ³ University of Science and Technology of China

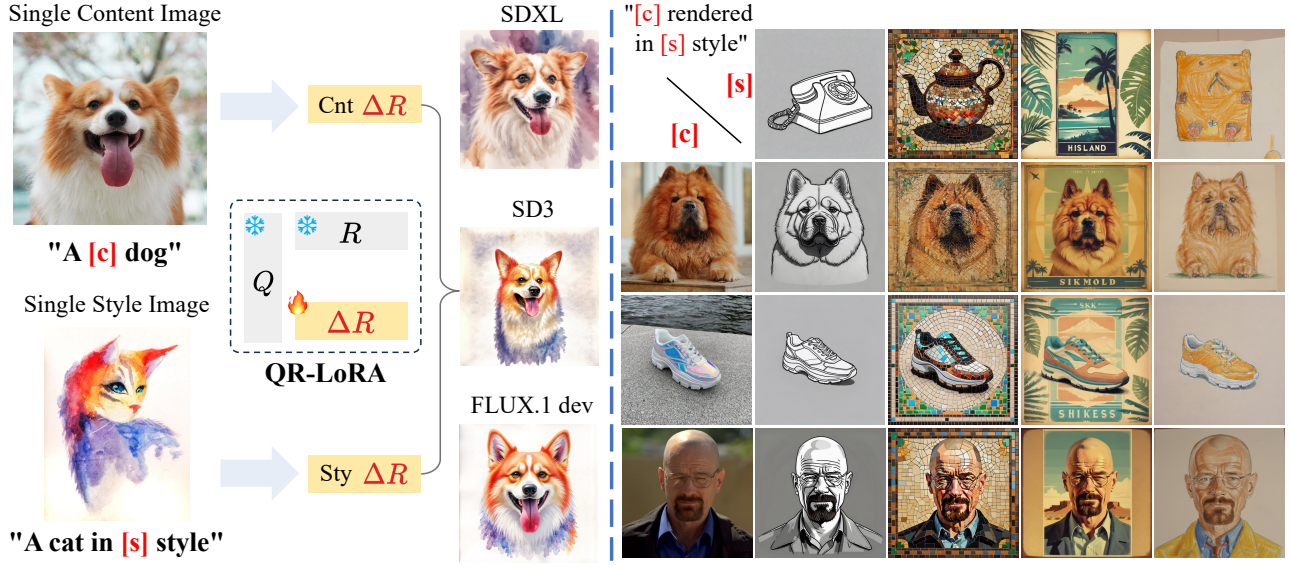


Figure 1. Given a single content and a single style image, we present **QR-LoRA**, a method to achieve efficient and disentangled control of content and style features through orthogonal decomposition. Our approach reduces trainable parameters while maintaining superior disentanglement properties, enabling flexible manipulation of visual attributes with enhanced initialization. **Best viewed with zoom-in.**

Abstract

Existing text-to-image models often rely on parameter fine-tuning techniques such as Low-Rank Adaptation (LoRA) to customize visual attributes. However, when combining multiple LoRA models for content-style fusion tasks, unstructured modifications of weight matrices often lead to undesired feature entanglement between content and style attributes. We propose **QR-LoRA**, a novel fine-tuning framework leveraging QR decomposition for structured parameter updates that effectively separate visual attributes. Our key insight is that the orthogonal Q matrix naturally minimizes interference between different visual features, while the upper triangular R matrix efficiently encodes attribute-specific transformations. Our approach fixes both Q and R matrices while only training an additional task-specific ΔR

matrix. This structured design reduces trainable parameters to half of conventional LoRA methods and supports effective merging of multiple adaptations without cross-contamination due to the strong disentanglement properties between ΔR matrices. Experiments demonstrate that **QR-LoRA** achieves superior disentanglement in content-style fusion tasks, establishing a new paradigm for parameter-efficient, disentangled fine-tuning in generative models.

1. Introduction

Feature disentanglement and control in generative models have been a long-standing challenge, particularly in the domain of image synthesis where precise manipulation of visual attributes is crucial for practical applications. Recent advances in diffusion models [16, 21, 34, 35, 40, 42, 47, 53, 54, 72, 73] have demonstrated remarkable capa-

^{*}Corresponding author

bilities in generating high-quality images. These models [6, 15, 18–20, 25, 44, 48, 52, 61, 72, 73] have shown impressive progress in both content generation and style manipulation, enabling diverse applications from photorealistic image synthesis to artistic style transfer. The rapid development of foundation models [16, 21, 53, 54, 68] and adaptation techniques [17, 38, 48, 72, 73] have made customizing generative models for specific visual tasks increasingly accessible, marking a milestone in AI-driven creative applications.

Contemporary approaches to feature disentanglement can be broadly categorized into content-specific [38, 48, 73], style-specific [15, 52, 61], and joint content-style methods [8, 31, 49]. While single-task approaches have shown success in their respective domains, the increasing demand for simultaneous control over both content and style has led to the development of more comprehensive solutions. Among various model adaptation techniques, Low-Rank Adaptation (LoRA) [17] has emerged as a particularly promising approach for its parameter efficiency and versatility. Yet, current joint content-style methods based on LoRA face significant challenges in achieving effective feature disentanglement while maintaining parameter efficiency. Recent solutions like ZipLoRA [49] attempt to achieve effective disentanglement by learning orthogonal coefficients between independently trained LoRAs, highlighting the importance of orthogonality in feature separation. However, such approaches, along with methods like B-LoRA [8], ComposLoRA [74], CMLoRA [76], remain heavily dependent on model-specific architectures [44, 47] and domain constraints. While the pursuit of orthogonality provides valuable insights for feature disentanglement, the field still lacks a unified, model-agnostic approach that can directly learn orthogonal adaptation modules without relying on post-training coefficient optimization.

In this paper, we introduce QR-LoRA, a novel fine-tuning framework that leverages QR decomposition [11] for disentangled content and style control. Our approach is motivated by both theoretical foundations and empirical observations. Through empirical analysis in Figure 2, we observe that Q matrices exhibit remarkably high similarity (approaching 1.0) across different adaptation tasks, while R matrices show relatively lower similarity. This stability of Q matrices is theoretically supported by the minimal Frobenius norm property of orthogonal parameterization (detailed in Appendix), which ensures that the orthogonal basis vectors maintain consistent orthogonality while minimizing redundant transformations in the feature space. Based on these insights, we propose a novel initialization paradigm that maintains Q as fixed orthogonal basis vectors spanning the linear transformation space, while introducing a ΔR mechanism to learn task-specific features, ensuring effective feature disentanglement while minimizing inter-

ference with the model’s original capabilities.

Our framework begins with singular value decomposition (SVD)-based [4, 10, 13, 29, 36, 50] core information extraction, followed by orthogonal basis construction through QR decomposition. The key innovation lies in our ΔR mechanism, which learns compact, task-specific transformations in the orthogonal space while preserving the model’s original capabilities. This approach not only achieves more precise feature disentanglement but also significantly reduces the number of trainable parameters. Unlike existing methods that rely on model-specific architectural analysis [8] or complex merging strategies for independently trained LoRAs [49], our method provides an elegant, model-agnostic solution that maintains consistent performance across various architectures. Extensive experiments demonstrate that QR-LoRA achieves superior disentanglement capabilities and faster convergence compared to conventional approaches, while requiring only half of the trainable parameters. Our main contributions are as follows:

- A novel SVD-QR based initialization paradigm for LoRA that constructs orthogonal basis vectors through matrix decomposition, reducing trainable parameters by half while maintaining model performance.
- A residual mechanism (ΔR) that learns task-specific transformations in a fixed orthogonal space, enabling precise control with disentanglement properties between visual attributes for effective merging.
- We demonstrate superior performance of QR-LoRA in content-style fusion tasks, with consistent results across various model architectures, highlighting its significant potential for broader applications.

2. Related Work

Parameter-Efficient Fine-tuning (PEFT) has emerged as a pivotal research area in large-scale generative models [28, 39, 64], particularly in adapting foundation models with minimal computational overhead. Various PEFT strategies have been proposed, including Adapter modules [55] that insert trainable layers, Prompt-tuning [27] that optimizes continuous prompts, and LoRA [17] that decomposes weight updates into low-rank matrices (*i.e.*, AB). Among these, LoRA has demonstrated remarkable success in large language models, inspiring innovative designs such as HydraLoRA [57] with asymmetric structures that leverage shared A matrices for global feature integration and task-specific B matrices for capturing intrinsic components, effectively minimizing interference between different tasks. Recent advances like PISSA [36] leverage SVD-based initialization for accelerated convergence, while SVDiff [13] introduces a compact parameter space by fine-tuning singular values of weight matrices, significantly reducing model size while maintaining performance.

SVFT [29] further advances the field by efficiently updating weights through sparse combinations of singular vectors, achieving remarkable performance with minimal trainable parameters. These advances in parameter-efficient learning have provided valuable insights for text-to-image model adaptation. However, the direct application of these techniques to visual generation tasks faces unique challenges due to the complex nature of visual feature disentanglement, especially in scenarios requiring fine-grained control over both content and style attributes.

Image customization in text-to-image models has evolved along several distinct technical trajectories. Model adaptation approaches [28, 31, 38, 49, 52, 72, 73] encompass various strategies from parameter-efficient modules to feature injection mechanisms and lightweight model adjustments, enabling flexible customization through different architectural modifications. Content-preserving methods [24, 48, 63, 72] emphasize maintaining subject identity and semantic consistency through specialized training strategies, introducing techniques for robust feature preservation and identity-aware generation. Advanced control mechanisms have emerged through attention-based techniques [1, 14, 15, 20, 24] and plug-and-play solutions [58], alongside lightweight training-free alternatives including editing-based approaches [3, 5, 7, 9, 19, 26, 37, 41, 61, 67] that enable flexible attribute manipulation through direct image editing and feature-level modifications without model re-training. Despite these developments, existing approaches face inherent limitations in achieving effective feature disentanglement while maintaining parameter efficiency, particularly when handling multiple customization objectives. These challenges stem from the complex nature of visual feature separation and the computational overhead required for precise attribute control, motivating our investigation into a more unified and parameter-efficient approach that leverages orthogonal basis vectors for disentanglement.

Feature disentanglement, particularly in the context of content and style separation, has been extensively studied in text-to-image models. Traditional approaches [38, 48, 73] focus on single-aspect control but struggle with joint manipulation of multiple attributes. Several methods have been proposed for merging multiple LoRA adaptations, such as Custom Diffusion [24], Mix-of-Show [12], Ortha [43], LoRACLR [51], they often require complex training strategies or additional regularization terms. In parallel, model-specific architectures [28, 49, 62] partially address this limitation through specialized designs for feature disentanglement, though their reliance on specific architectural choices limits their generality, with methods like B-LoRA [8] leveraging SDXL’s architectural characteristics to identify specific blocks crucial for style-content separation, and ZipLoRA [49] proposing efficient merging strategies for independently trained style and subject LoRAs. While

these approaches demonstrate promising results within their targeted frameworks, they remain heavily dependent on model-specific architectures (particularly SDXL) and often face challenges in maintaining both subject and style fidelity during joint generation.

3. Method

3.1. Preliminaries

Continuous generative frameworks. Modern generative models often construct samples through learned continuous dynamics that bridge data distributions and tractable priors. Two prominent paradigms—diffusion models [16, 44, 47, 54] and flow matching [6, 25, 30, 32], share this philosophy but differ in their construction of probability paths and training objectives. Both frameworks leverage continuous transformations to map between a complex data distribution and a simple prior distribution, enabling efficient sampling and learning. Diffusion models gradually corrupt observed data \mathbf{x} by mixing it with Gaussian noise (ϵ) over time: $\mathbf{z}_t = \alpha_t \mathbf{x} + \sigma_t \epsilon$. The goal is to learn a reverse process that can reconstruct the original data from the noisy samples. Training involves estimating either $\hat{\mathbf{x}}$ or $\hat{\epsilon}$ using a neural network:

$$\mathcal{L}(\mathbf{x}) = \mathbb{E}_{t \sim \mathcal{U}(0,1), \epsilon \sim \mathcal{N}(0, \mathbf{I})} \left[w(\lambda_t) \cdot \frac{d\lambda}{dt} \cdot \|\hat{\epsilon} - \epsilon\|_2^2 \right], \quad (1)$$

where $\lambda_t = \log(\alpha_t^2 / \sigma_t^2)$ is the log signal-to-noise ratio, and $w(\lambda_t)$ is a weighting function that balances the importance of different noise levels [22]. Flow matching views the forward process as a linear interpolation between the data \mathbf{x} and a noise term ϵ : $\mathbf{z}_t = (1 - t)\mathbf{x} + t\epsilon$. The key idea is to learn a velocity field \mathbf{u}_t that describes the continuous transformation from noise to data:

$$\mathcal{L}_{\text{CFM}}(\mathbf{x}) = \mathbb{E}_{t \sim \mathcal{U}(0,1), \epsilon \sim \mathcal{N}(0, \mathbf{I})} [\|\hat{\mathbf{u}} - \mathbf{u}\|_2^2], \quad (2)$$

where $\hat{\mathbf{u}}$ is the predicted velocity field, which can be expressed as a linear combination of $\hat{\epsilon}$ and \mathbf{z}_t . This objective can be rewritten in terms of the noise prediction, similar to Eq. 1, with an appropriate weighting function.

LoRA fine-tuning. LoRA has emerged as a parameter-efficient fine-tuning approach for adapting large pre-trained models to downstream tasks. Given a pre-trained weight matrix $W \in \mathbb{R}^{m \times n}$, LoRA learns a low-rank update $\Delta W = BA$, where $B \in \mathbb{R}^{m \times r}$ and $A \in \mathbb{R}^{r \times n}$ are trainable matrices with rank $r \ll \min(m, n)$. This decomposition significantly reduces the number of trainable parameters from mn to $r(m + n)$. In text-to-image models [6, 25, 44], LoRA is typically injected into key components such as cross-attention and self-attention [59] layers, we provide detailed injection configurations in the Appendix. During training, the original objective functions (*i.e.*, Eq. 1 or Eq. 2) remain unchanged, but the optimization is performed only on the

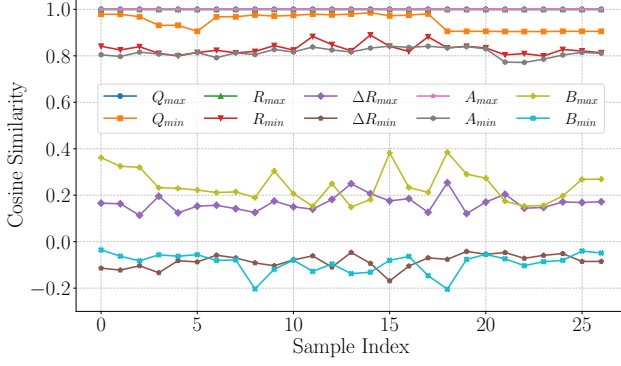


Figure 2. **Maximum and minimum cosine similarities across different matrices.** Q and R matrices are obtained from QR-LoRA framework with direct fine-tuning strategy, ΔR matrices from QR-LoRA framework with ΔR -only update strategy, and A , B matrices from vanilla LoRA decomposition. The analysis reveals distinct similarity patterns across these matrix types, demonstrating their unique roles in feature representation. All similarity values are computed between matrices trained on different image pairs. See Appendix for experimental cases and training details.

low-rank parameters A and B , while keeping the pretrained weights W fixed, as shown in Figure 4 (b).

3.2. Motivation and Analysis

Existing methods like ZipLoRA [49], ComposLoRA [74], and CMLoRA [76], while maintaining the original LoRA [17] training paradigm, share a common approach: they first train independent LoRA modules with the standard structure and then focus on studying their merging strategies. However, is this paradigm the optimal approach? This raises a fundamental question: *Could we redesign the LoRA structure from the ground up to achieve inherent feature disentanglement and better merging capabilities?* Through extensive matrix similarity analysis, we identify two critical insights that motivate our approach:

Feature entanglement in direct weight updates. The conventional LoRA training paradigm and direct QR decomposition training both exhibit similar feature entanglement issues. Our analysis reveals high cosine similarities between task-specific updates (Figure 2), particularly in the matrices A and Q . While the B matrices show relatively lower similarities, the R matrices demonstrate notably higher similarities (> 0.75) due to our initialization strategy that inherits substantial prior information from the original weights (detailed in Algorithm 1 and Sec 3.3). This similarity pattern reveals a crucial insight: the stability of Q matrices across different tasks suggests their potential as fixed orthogonal bases, while the R matrices provides suitable flexibility for task-specific adaptations. Since both approaches require training multiple components (*i.e.*, A, B and Q, R), achieving clean feature separation during merg-

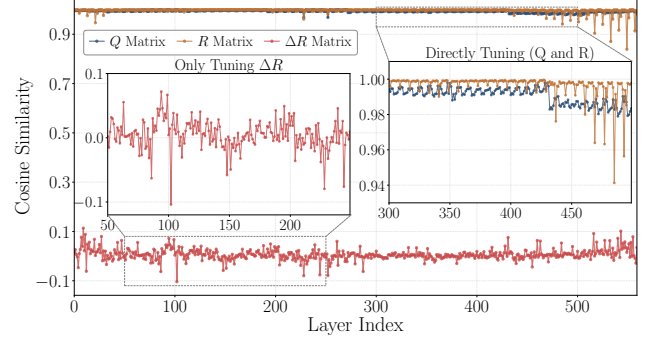


Figure 3. **Comparison of cosine similarities between different training strategies in QR-LoRA.** Visualization of layer-wise cosine similarities between matrices obtained from training on a randomly selected image pair in SDXL model. The comparison demonstrates distinct characteristics between directly fine-tuning Q and R matrices (upper zoom-in) versus only tuning ΔR matrices (lower zoom-in). See Appendix for comprehensive analyses across different model architectures and training data.

ing becomes challenging. This observation motivates our design choice to focus on learning task-specific updates ΔR rather than training the entire decomposition. The effectiveness of this approach is validated by our empirical results in Figure 2 and Figure 3, which show that the maximum cosine similarity between ΔR matrices across all injection layers remains consistently below 0.2, with mean values stable around 0, indicating superior feature disentanglement.

Lack of structural constraints. Most existing methods treat weight updates as unconstrained matrices, without leveraging mathematical properties that could facilitate feature disentanglement. Our investigation shows that imposing appropriate structural constraints through matrix decomposition can lead to more effective feature separation. Specifically, we find that orthogonal bases provide a natural framework for maintaining feature independence while allowing flexible combinations (see Appendix for detailed theoretical analysis). Inspired by these observations and the properties revealed in Figure 2 and Figure 3, we propose to leverage QR decomposition’s unique characteristics. The orthogonal matrix Q provides an ideal basis for representing features independently, while the upper triangular matrix R captures the essential transformations. This enables us to design a novel LoRA variant that naturally preserves feature disentanglement from the outset, rather than attempting to achieve it through post-training merging strategies.

3.3. QR-LoRA Methodology

Based on our analysis of the limitations in existing approaches and the insights gained from matrix similarity studies, we propose QR-LoRA, a novel parameter-efficient fine-tuning framework that naturally facilitates feature disentanglement through orthogonal decomposition. The key

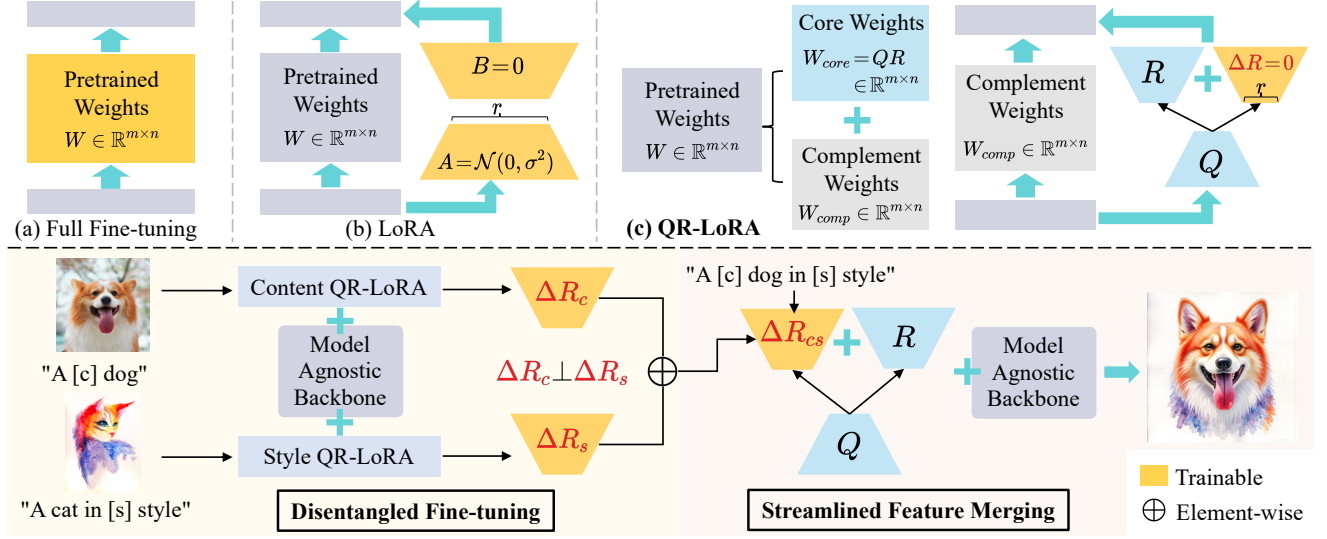


Figure 4. **Overview of QR-LoRA framework.** Upper (Sec 3.3): Technical illustration of our method compared to traditional fine-tuning paradigms, highlighting our efficient parameter updates through orthogonal decomposition. Lower (Sec 3.4): Application pipeline of our framework for content-style disentanglement, consisting of a disentangled fine-tuning module and a streamlined feature merging module.

innovation of our approach lies in its unique initialization strategy and training mechanism, which we detail below.

Core information extraction. As illustrated in the upper part of Figure 4, compared to traditional full fine-tuning and LoRA, our QR-LoRA achieves more efficient parameter updates through orthogonal decomposition. Given a pretrained weight matrix $W \in \mathbb{R}^{m \times n}$, we first employ SVD to systematically extract its core information structure (Figure 4 (c)). This decomposition provides a natural way to identify and isolate the most significant components of the weight matrix:

$$W = U\Sigma V^\top = \sigma_1 u_1 v_1^\top + \sigma_2 u_2 v_2^\top + \dots + \sigma_s u_s v_s^\top, \quad (3)$$

where $s = \min(m, n)$, $U \in \mathbb{R}^{m \times s}$ contains the left singular vectors, $\Sigma \in \mathbb{R}^{s \times s}$ is a diagonal matrix of singular values arranged in descending order ($\sigma_1 \geq \sigma_2 \geq \dots \geq \sigma_s$), reflecting the decreasing importance of feature dimensions, and $V^\top \in \mathbb{R}^{s \times n}$ contains the right singular vectors. By leveraging this natural ordering where larger singular values correspond to more significant feature transformations, we can construct a reduced- r core matrix that captures the most essential feature transformations:

$$W_{core} = U_{[:,r]} \Sigma_{[r]} V_{[r,:]}^\top \triangleq \sigma_1 u_1 v_1^\top + \dots + \sigma_r u_r v_r^\top, \quad (4)$$

this strategic truncation yields two complementary components: the core matrix W_{core} that encapsulates the dominant feature transformations, and a complement matrix $W_{comp} = W - W_{core}$ that retains the residual information. This decomposition serves a dual purpose: it ensures that our subsequent QR-based adaptation focuses on the most significant components while maintaining structural consistency with the original LoRA framework through the ini-

tialization of the pretrained weight matrix W with W_{comp} , which is outlined in Algorithm 1 lines 1-4.

Orthogonal basis construction. To effectively capture and manipulate feature transformations, we leverage QR decomposition to construct orthogonal bases for our parameter updates. Rather than directly decomposing W_{core} , we strategically apply QR decomposition to its transpose W_{core}^\top , which aligns with our goal of maintaining consistent matrix multiplication order with the original LoRA formulation ($\Delta W = BA \Leftrightarrow R^\top Q^\top$). Given that $W_{core}^\top = V_{[r,:]} \Sigma_{[r]} U_{[:,r]}^\top$, we can naturally express it as a product of two low-rank matrices (S and T):

$$\begin{aligned} W_{core}^\top &= \underbrace{V_{[r,:]} \Sigma_{[r]}}_S \underbrace{U_{[:,r]}^\top}_T = (Q_s R_s) T \\ &= \underbrace{Q_s}_Q \underbrace{(R_s T)}_R \triangleq QR, \end{aligned} \quad (5)$$

where S characterizes the core structure of the column space of W_{core}^\top . By performing reduced QR decomposition ($Q_s R_s$) on S rather than the full matrix, we obtain more precise orthogonal bases while maintaining computational efficiency. Through initializing the task-specific update matrix ΔR to zero, the final initialization of our QR-LoRA framework takes the form:

$$W_{origin} = W_{comp} + (Q(R + \Delta R))^\top, \quad (6)$$

where W_{origin} represents the original pretrained weights. By keeping both Q and R fixed during training, we provide stable anchors for task-specific adaptations through ΔR . The complete process is detailed in Algorithm 1.

3.4. Task-Specific Training

As illustrated in the lower part of Figure 4, we apply our QR-LoRA framework to the challenging task of content-style disentanglement in image generation. Our approach consists of two key components that leverage the inherent orthogonality properties of our framework:

Disentangled fine-tuning. Through efficient fine-tuning on individual images, we separately learn content-specific (ΔR_c) and style-specific (ΔR_s) update matrices. The orthogonal basis Q provided by our framework naturally facilitates this disentanglement by ensuring that different feature transformations remain independent (*i.e.*, $\Delta R_c \perp \Delta R_s$ as shown in Figure 2). This independence is further reinforced by our training strategy where each ΔR matrix is optimized for its specific task (*e.g.*, content or style) while maintaining the shared orthogonal basis Q and base matrix R fixed.

Streamlined feature merging. The inherent disentanglement properties of our learned ΔR matrices enable a remarkably simple yet effective merging strategy. Unlike existing approaches that require complex merging mechanisms, our method achieves flexible content-style integration through straightforward element-wise addition of the update matrices:

$$\Delta R_{cs} = \lambda_c \Delta R_c + \lambda_s \Delta R_s \quad (7)$$

where λ_c and λ_s are scaling coefficients that provide fine-grained control over the contribution of content and style features in the final generation. By default, $\lambda_c = \lambda_s = 1$.

4. Experiments

4.1. Implementation details

Experimental setup. To validate the model-agnostic nature of our framework, we evaluate QR-LoRA on multiple state-of-the-art diffusion models including SDXL [44], SD3 [6], and FLUX.1-dev [25]. During the fine-tuning process, we keep the pretrained model weights and text encoders frozen. All experiments are conducted on a single image per training instance. We employ the Adam [23] optimizer with a learning rate of $1e-4$ without data augmentations. The LoRA rank is set to $r = 64$ with 500 training steps, requiring approximately 20 minutes on a single A800 GPU. Our training data is sourced from previous works [48, 52, 65] and publicly available content. Following previous works [48, 49, 52], we adopt a standard prompt template for training. Specifically, we use $\langle c \rangle$ to denote content-related trigger words (*e.g.*, “[c]” or “sks”) and $\langle s \rangle$ for style-related expressions (*e.g.*, “[s]” or simple artistic description [28, 49]), combining them in the format “a $\langle c \rangle$ in $\langle s \rangle$ style”. For fair comparison, we maintain consistent content and style image settings across all comparative experiments.

Compared methods. For SDXL [44], where most recent style transfer methods are developed, we compare against state-of-the-art approaches including ZipLoRA

Algorithm 1: QR-LoRA for Efficient and Disentangled Fine-tuning with Orthogonal Basis

Input: Pretrained weight matrix $W \in \mathbb{R}^{m \times n}$;
Target task type τ (content or style);
Rank r for low-rank approximation; Learning rate η
Output: Trained ΔR_τ ; Orthogonal basis Q ;
Upper triangular base matrix R

```

1  $U, \Sigma, V^\top \leftarrow \text{SVD}(W)$  // SVD of  $W$ 
2  $W_{core} \leftarrow U_{[:,r]} \Sigma_{[r,r]} V_{[r,:]}^\top$  // Core matrix
3  $W_{comp} \leftarrow W - W_{core}; W_{origin} \leftarrow W$ 
4  $W \leftarrow W_{comp}$  // Complement matrix
5  $S \leftarrow V_{[r,:]} \Sigma_{[r,r]} \in \mathbb{R}^{n \times r}; T \leftarrow U_{[r,:]}^\top \in \mathbb{R}^{r \times m}$ 
6  $Q_s, R_s \leftarrow \text{QR}(S); Q_s \in \mathbb{R}^{n \times r}, R_s \in \mathbb{R}^{r \times r}$ 
   // Reduced QR decomposition
7  $Q \leftarrow Q_s; R \leftarrow R_s T \in \mathbb{R}^{r \times m}$ 
8 Initialize  $\Delta R_\tau \leftarrow 0_{r \times m}$  // Init to zero
9  $W_{origin} = W_{comp} + (Q(R + \Delta R))^\top$ 
10 while not converged do
11    $\mathcal{L} \leftarrow \text{TaskLoss}\{W_{comp} + (Q(R + \Delta R_\tau))^\top\}$ 
    $\Delta R_\tau \leftarrow \Delta R_\tau - \eta \nabla_{\Delta R_\tau} \mathcal{L}$  // Update
12 return  $\Delta R_\tau, Q, R$ 

```

[49], StyleAligned [15], and B-LoRA [28]. For SD3 [6] and FLUX.1-dev [25] models, we compare against DreamBooth-LoRA [60] using naive weight combination.

Metrics. To evaluate our method quantitatively, we compute cosine similarities between generated images and their references using DINO [2] and CLIP [45] features for both style (-S) and content (-C) aspects. We also conduct a user study to assess the perceptual quality, with detailed settings provided in the Appendix.

4.2. Results and Analysis

We conduct comprehensive quantitative and qualitative experiments to evaluate our method, with additional experimental results provided in the supplementary material.

Qualitative Analysis. Figure 5 demonstrates the superior performance of QR-LoRA across various test scenarios. Our method consistently outperforms existing approaches in style transfer tasks, with particularly notable advantages in preserving human poses and anatomical details when handling complex body structures and dynamic postures. Moreover, QR-LoRA exhibits strong model-agnostic capabilities, achieving consistent high-quality results across different backbone models including SDXL, SD3, and FLUX.1-dev, which is also demonstrated in Figure 6. This cross-model effectiveness demonstrates that our approach to feature manipulation and style transfer can be successfully applied to diverse model architectures while maintaining structural integrity of the generated images.

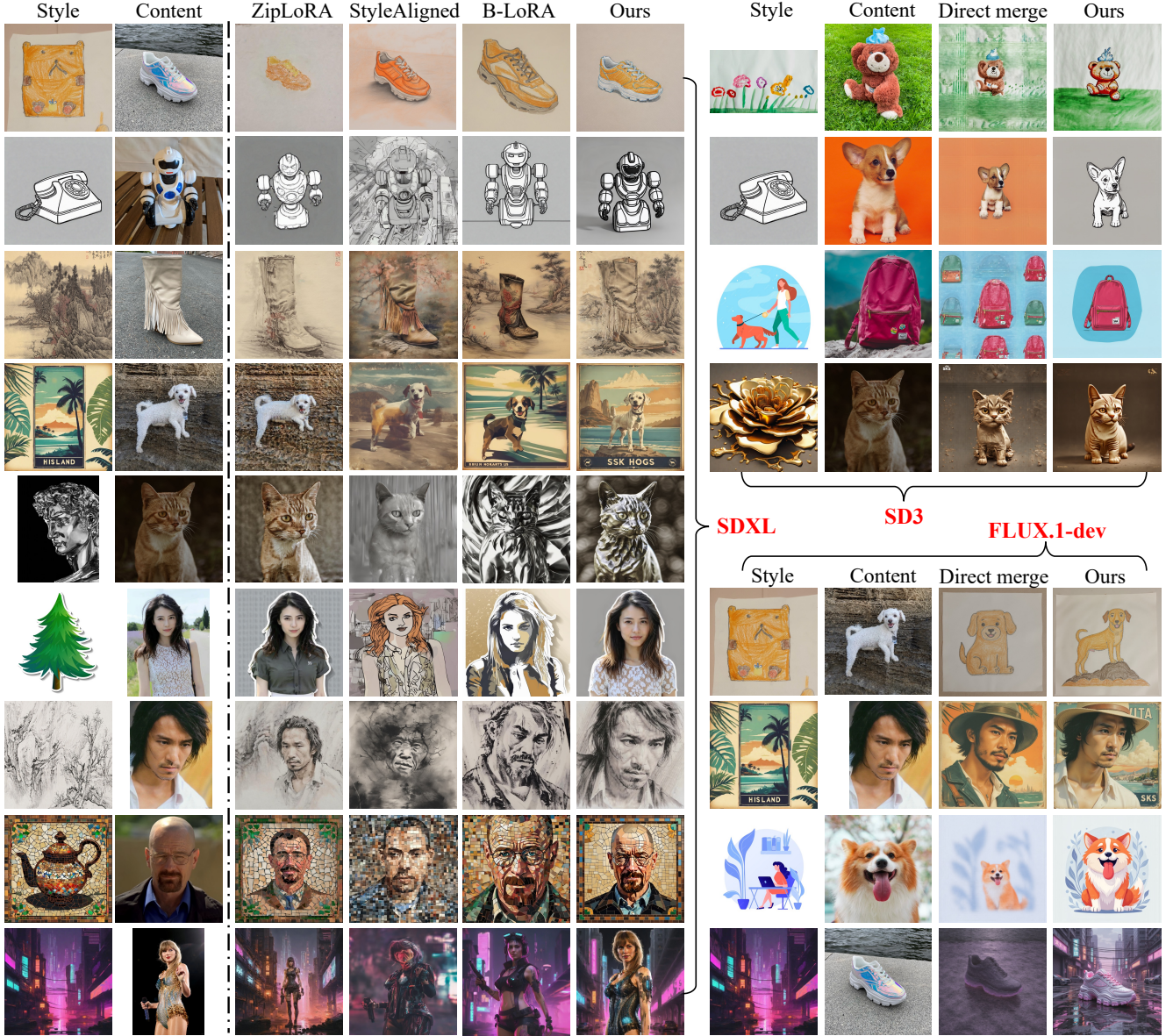


Figure 5. **Qualitative comparison.** Comparison of our QR-LoRA against state-of-the-art methods on SDXL and a naive baseline on SD3 and FLUX.1-dev models, demonstrating the model-agnostic nature and superior performance of our framework. Zoom in to view details.

Table 1. Quantitative comparison across different backbone models (SDXL, SD3, FLUX.1-dev). We report cosine similarities between generated images and their style (-S) or content (-C) references using DINO and CLIP features, along with user ratings (0-5 scale).

	SDXL [44]				SD3 [6]		FLUX.1-dev [25]	
	ZipLoRA [49]	B-LoRA [28]	StyleAligned [15]	Ours	DB-LoRA [60]	Ours	DB-LoRA [60]	Ours
DINO-S [2] ↑	0.686 ± 0.131	0.689 ± 0.075	0.651 ± 0.061	0.694 ± 0.084	0.675 ± 0.043	0.711 ± 0.061	0.723 ± 0.105	0.744 ± 0.077
DINO-C [2] ↑	0.712 ± 0.112	0.740 ± 0.064	0.758 ± 0.053	0.776 ± 0.065	0.673 ± 0.032	0.690 ± 0.040	0.654 ± 0.072	0.687 ± 0.086
CLIP-S [45] ↑	0.686 ± 0.105	0.669 ± 0.085	0.658 ± 0.076	0.707 ± 0.060	0.652 ± 0.071	0.703 ± 0.056	0.641 ± 0.074	0.690 ± 0.069
CLIP-C [45] ↑	0.668 ± 0.149	0.646 ± 0.098	0.662 ± 0.114	0.709 ± 0.087	0.771 ± 0.081	0.792 ± 0.077	0.677 ± 0.125	0.709 ± 0.096
User-Study ↑	3.13	3.34	3.67	4.07	2.93	4.14	2.86	3.96

Quantitative Analysis We evaluate our method on a test set of 64 randomly sampled generated images. As shown in Table 1, QR-LoRA outperforms state-of-the-art methods on SDXL in both content preservation and style transfer,

with significantly higher user ratings in our user study. On SD3 and FLUX.1-dev, our method consistently improves over the naive baseline DB-LoRA [60] (*i.e.*, direct merge), demonstrating its model-agnostic effectiveness.



Figure 6. **Visualization on different backbone models.** Demonstration of QR-LoRA’s generation results across different backbone models, showing consistent high-quality performance.

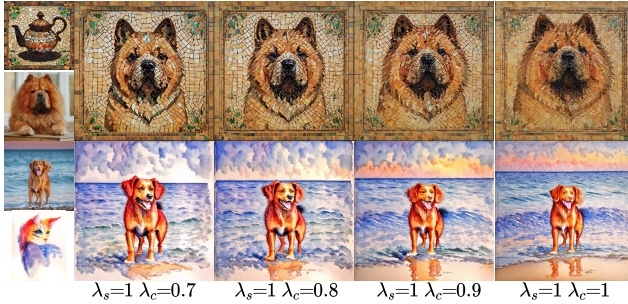


Figure 7. **Ablation study** on scaling coefficient λ_c and λ_s .

Ablation. To further validate the robustness of our method, we experiment with different combinations of scaling coefficients λ_c and λ_s during feature composition. As shown in Figure 7, the consistent high-quality results across various coefficient pairs demonstrate that our approach is inherently robust, indicating that this scaling flexibility is a natural property rather than a requirement of our method.

4.3. Application

Adaptive Training Strategies. Our framework provides flexible training configurations for different scenarios as shown in Figure 8. For feature disentanglement tasks, training only the ΔR matrices achieves comparable convergence to standard LoRA with better generalization. When faster convergence is needed, training both Q and R components simultaneously accelerates the process by leveraging pre-trained structural information.

Versatile Feature Composition. Beyond style-content synthesis, our method demonstrates remarkable capability in disentangled composition of various image attributes. As shown in Figure 9, QR-LoRA effectively handles diverse feature combinations. This versatility highlights the method’s potential for broader applications.



Figure 8. **Convergence analysis.** Comparison of training convergence between QR-LoRA and LoRA.

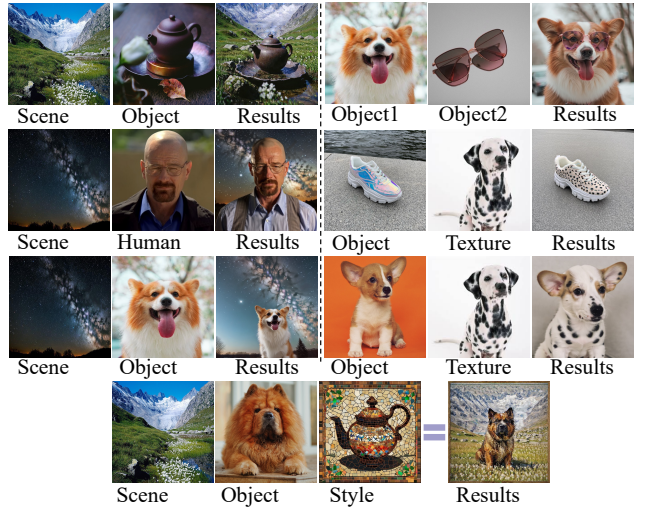


Figure 9. **Applications on multi-feature composition.** Our method enables flexible combination of various image attributes, demonstrating its capability beyond style-content synthesis.

5. Discussion

In this work, we have proposed QR-LoRA, a novel parameter-efficient fine-tuning framework that achieves effective feature disentanglement through orthogonal decomposition. By leveraging SVD-QR based initialization and a ΔR mechanism in a fixed orthogonal space, our approach reduces trainable parameters while enabling precise feature control. The framework demonstrates robust performance across different architectures, offering a complementary solution for feature disentanglement tasks.

Limitation. While our method demonstrates strong performance, the incorporation of matrix decomposition operations during initialization introduces additional computational overhead. Specifically, this initialization process requires $\sim 1, 2,$ and 5 minutes for SDXL, SD3, and FLUX.1-dev respectively. However, this one-time cost during initialization does not affect subsequent inference efficiency.

Future Work. The model-agnostic nature of QR-LoRA

enables its extension to other modalities such as 3D [46, 66] and video [56, 69–71, 75] customization. Furthermore, our framework naturally aligns with Mixture-of-Experts (MoE) [33] architectures when extended to multiple ΔR matrices, where studying the collaborative dynamics could enable more flexible and powerful control capabilities.

References

- [1] Yuval Alaluf, Daniel Garibi, Or Patashnik, Hadar Averbuch-Elor, and Daniel Cohen-Or. Cross-image attention for zero-shot appearance transfer. In *ACM SIGGRAPH 2024 Conference Papers*, pages 1–12, 2024. 3
- [2] Mathilde Caron, Hugo Touvron, Ishan Misra, Hervé Jégou, Julien Mairal, Piotr Bojanowski, and Armand Joulin. Emerging properties in self-supervised vision transformers. In *Proceedings of the IEEE/CVF international conference on computer vision*, pages 9650–9660, 2021. 6, 7
- [3] Minghao Chen, Iro Laina, and Andrea Vedaldi. Training-free layout control with cross-attention guidance. *arXiv preprint arXiv:2304.03373*, 2023. 3
- [4] Carl Eckart and Gale Young. The approximation of one matrix by another of lower rank. *Psychometrika*, 1(3):211–218, 1936. 2
- [5] Dave Epstein, Allan Jabri, Ben Poole, Alexei Efros, and Aleksander Holynski. Diffusion self-guidance for controllable image generation. *Advances in Neural Information Processing Systems*, 36:16222–16239, 2023. 3
- [6] Patrick Esser, Sumith Kulal, Andreas Blattmann, Rahim Entezari, Jonas Müller, Harry Saini, Yam Levi, Dominik Lorenz, Axel Sauer, Frederic Boesel, et al. Scaling rectified flow transformers for high-resolution image synthesis. In *Forty-first International Conference on Machine Learning*, 2024. 2, 3, 6, 7
- [7] Farzad Farhadzadeh, Debasmit Das, Shubhankar Borse, and Fatih Porikli. Lora-x: Bridging foundation models with training-free cross-model adaptation. In *ICLR*, 2025. 3
- [8] Yarden Frenkel, Yael Vinker, Ariel Shamir, and Daniel Cohen-Or. Implicit style-content separation using b-lora. In *European Conference on Computer Vision*, pages 181–198. Springer, 2025. 2, 3, 15
- [9] Rinon Gal, Yuval Alaluf, Yuval Atzmon, Or Patashnik, Amit H Bermano, Gal Chechik, and Daniel Cohen-Or. An image is worth one word: Personalizing text-to-image generation using textual inversion. *arXiv preprint arXiv:2208.01618*, 2022. 3
- [10] Gene H Golub and Christian Reinsch. Singular value decomposition and least squares solutions. In *Handbook for Automatic Computation: Volume II: Linear Algebra*, pages 134–151. Springer, 1971. 2
- [11] Gene H Golub and Charles F Van Loan. Matrix computations. Johns hopkins university press. *Baltimore and London*, 41: 62, 1996. 2
- [12] Yuchao Gu, Xintao Wang, Jay Zhangjie Wu, Yujun Shi, Chen Yunpeng, Zihan Fan, Wuyou Xiao, Rui Zhao, Shuning Chang, Weijia Wu, Yixiao Ge, Shan Ying, and Mike Zheng Shou. Mix-of-show: Decentralized low-rank adaptation for multi-concept customization of diffusion models. *NeurIPS*, 2023. 3
- [13] Ligong Han, Yinxiao Li, Han Zhang, Peyman Milanfar, Dimitris Metaxas, and Feng Yang. Svdif: Compact parameter space for diffusion fine-tuning. In *Proceedings of the IEEE/CVF International Conference on Computer Vision*, pages 7323–7334, 2023. 2
- [14] Amir Hertz, Ron Mokady, Jay Tenenbaum, Kfir Aberman, Yael Pritch, and Daniel Cohen-Or. Prompt-to-prompt image editing with cross attention control. *arXiv preprint arXiv:2208.01626*, 2022. 3
- [15] Amir Hertz, Andrey Voynov, Shlomi Fruchter, and Daniel Cohen-Or. Style aligned image generation via shared attention. In *Proceedings of the IEEE/CVF Conference on Computer Vision and Pattern Recognition*, pages 4775–4785, 2024. 2, 3, 6, 7
- [16] Jonathan Ho, Ajay Jain, and Pieter Abbeel. Denoising diffusion probabilistic models. In *NeurIPS*, pages 6840–6851, 2020. 1, 2, 3
- [17] Edward J Hu, Yelong Shen, Phillip Wallis, Zeyuan Allen-Zhu, Yuanzhi Li, Shean Wang, Lu Wang, and Weizhu Chen. Lora: Low-rank adaptation of large language models. *arXiv preprint arXiv:2106.09685*, 2021. 2, 4, 12, 13
- [18] Ajay Jain, Ben Mildenhall, Jonathan T Barron, Pieter Abbeel, and Ben Poole. Zero-shot text-guided object generation with dream fields. In *CVPR*, pages 867–876, 2022. 2
- [19] Geonhui Jang, Jin-Hwa Kim, Yong-Hyun Park, Junho Kim, Gayoung Lee, and Yonghyun Jeong. Decor:decomposition and projection of text embeddings for text-to-image customization, 2024. 3
- [20] Jaeseok Jeong, Junho Kim, Yunjey Choi, Gayoung Lee, and Youngjung Uh. Visual style prompting with swapping self-attention. *arXiv preprint arXiv:2402.12974*, 2024. 2, 3
- [21] Tero Karras, Miika Aittala, Timo Aila, and Samuli Laine. Elucidating the design space of diffusion-based generative models. In *NeurIPS*, pages 26565–26577, 2022. 1, 2
- [22] Diederik Kingma and Ruiqi Gao. Understanding diffusion objectives as the elbo with simple data augmentation. *Advances in Neural Information Processing Systems*, 36, 2024. 3
- [23] Diederik P Kingma. Adam: A method for stochastic optimization. *arXiv preprint arXiv:1412.6980*, 2014. 6
- [24] Nupur Kumari, Bingliang Zhang, Richard Zhang, Eli Shechtman, and Jun-Yan Zhu. Multi-concept customization of text-to-image diffusion. In *Proceedings of the IEEE/CVF Conference on Computer Vision and Pattern Recognition (CVPR)*, 2023. 3
- [25] Black Forest Labs. Flux. <https://github.com/black-forest-labs/flux>, 2023. 2, 3, 6, 7
- [26] Mingkun Lei, Xue Song, Beier Zhu, Hao Wang, and Chi Zhang. Stylestudio: Text-driven style transfer with selective control of style elements. In *CVPR*, 2025. 3
- [27] Brian Lester, Rami Al-Rfou, and Noah Constant. The power of scale for parameter-efficient prompt tuning. *arXiv preprint arXiv:2104.08691*, 2021. 2

- [28] Yang Li, Shaobo Han, and Shihao Ji. Vb-lora: Extreme parameter efficient fine-tuning with vector banks. In *The 38th Conference on Neural Information Processing Systems (NeurIPS)*, 2024. 2, 3, 6, 7
- [29] Vijay Lingam, Atula Tejaswi, Aditya Vavre, Aneesh Shetty, Gautham Krishna Gudur, Joydeep Ghosh, Alex Dimakis, Eunsol Choi, Aleksandar Bojchevski, and Sujay Sanghavi. Svft: Parameter-efficient fine-tuning with singular vectors. *arXiv preprint arXiv:2405.19597*, 2024. 2, 3
- [30] Yaron Lipman, Ricky TQ Chen, Heli Ben-Hamu, Maximilian Nickel, and Matt Le. Flow matching for generative modeling. *arXiv preprint arXiv:2210.02747*, 2022. 3
- [31] Chang Liu, Viraj Shah, Aiyu Cui, and Svetlana Lazebnik. Unziplora: Separating content and style from a single image. *arXiv preprint arXiv:2412.04465*, 2024. 2, 3
- [32] Xingchao Liu, Chengyue Gong, and Qiang Liu. Flow straight and fast: Learning to generate and transfer data with rectified flow. *arXiv preprint arXiv:2209.03003*, 2022. 3
- [33] Zefang Liu and Jiahua Luo. Adamole: Fine-tuning large language models with adaptive mixture of low-rank adaptation experts. *arXiv preprint arXiv:2405.00361*, 2024. 9
- [34] Yongjia Ma, Junlin Chen, Donglin Di, Qi Xie, Lei Fan, Wei Chen, Xiaofei Gou, Na Zhao, and Xun Yang. Tuning-free long video generation via global-local collaborative diffusion, 2025. 1
- [35] Yongjia Ma, Donglin Di, Xuan Liu, Xiaokai Chen, Lei Fan, Wei Chen, and Tonghua Su. Adams bashforth moulton solver for inversion and editing in rectified flow, 2025. 1
- [36] Fanxu Meng, Zhaohui Wang, and Muhan Zhang. Pissa: Principal singular values and singular vectors adaptation of large language models. In *NeurIPS*, 2024. 2
- [37] Ron Mokady, Amir Hertz, Kfir Aberman, Yael Pritch, and Daniel Cohen-Or. Null-text inversion for editing real images using guided diffusion models. In *Proceedings of the IEEE/CVF Conference on Computer Vision and Pattern Recognition*, pages 6038–6047, 2023. 3
- [38] Chong Mou, Xintao Wang, Liangbin Xie, Yanze Wu, Jian Zhang, Zhongang Qi, and Ying Shan. T2i-adapter: Learning adapters to dig out more controllable ability for text-to-image diffusion models. In *Proceedings of the AAAI Conference on Artificial Intelligence*, pages 4296–4304, 2024. 2, 3
- [39] Yao Ni, Shan Zhang, and Piotr Koniusz. PACE: marrying the generalization of PArmeter-efficient fine-tuning with consistency regularization. In *The Thirty-eighth Annual Conference on Neural Information Processing Systems*, 2024. 2
- [40] Alexander Quinn Nichol and Prafulla Dhariwal. Improved denoising diffusion probabilistic models. pages 8162–8171. PMLR, 2021. 1
- [41] Haowen Pan, Yixin Cao, Xiaozhi Wang, Xun Yang, and Meng Wang. Finding and editing multi-modal neurons in pre-trained transformers. In *Findings of the Association for Computational Linguistics ACL 2024*, pages 1012–1037, Bangkok, Thailand and virtual meeting, 2024. Association for Computational Linguistics. 3
- [42] William Peebles and Saining Xie. Scalable diffusion models with transformers. In *ICCV*, pages 4195–4205, 2023. 1
- [43] Ryan Po, Guandao Yang, Kfir Aberman, and Gordon Wetzstein. Orthogonal adaptation for modular customization of diffusion models. In *Proceedings of the IEEE/CVF Conference on Computer Vision and Pattern Recognition*, pages 7964–7973, 2024. 3, 12, 13
- [44] Dustin Podell, Zion English, Kyle Lacey, Andreas Blattmann, Tim Dockhorn, Jonas Müller, Joe Penna, and Robin Rombach. Sdxl: Improving latent diffusion models for high-resolution image synthesis. *arXiv preprint arXiv:2307.01952*, 2023. 2, 3, 6, 7
- [45] Alec Radford, Jong Wook Kim, Chris Hallacy, Aditya Ramesh, Gabriel Goh, Sandhini Agarwal, Girish Sastry, Amanda Askell, Pamela Mishkin, Jack Clark, et al. Learning transferable visual models from natural language supervision. In *International conference on machine learning*, pages 8748–8763. PMLR, 2021. 6, 7
- [46] Amit Raj, Srinivas Kaza, Ben Poole, Michael Niemeyer, Nataniel Ruiz, Ben Mildenhall, Shiran Zada, Kfir Aberman, Michael Rubinstein, Jonathan Barron, et al. Dreambooth3d: Subject-driven text-to-3d generation. In *CVPR*, pages 2349–2359, 2023. 9
- [47] Robin Rombach, Andreas Blattmann, Dominik Lorenz, Patrick Esser, and Björn Ommer. High-resolution image synthesis with latent diffusion models. In *CVPR*, pages 10684–10695, 2022. 1, 2, 3
- [48] Nataniel Ruiz, Yuanzhen Li, Varun Jampani, Yael Pritch, Michael Rubinstein, and Kfir Aberman. Dreambooth: Fine tuning text-to-image diffusion models for subject-driven generation. In *Proceedings of the IEEE/CVF conference on computer vision and pattern recognition*, pages 22500–22510, 2023. 2, 3, 6
- [49] Viraj Shah, Nataniel Ruiz, Forrester Cole, Erika Lu, Svetlana Lazebnik, Yuanzhen Li, and Varun Jampani. Ziplora: Any subject in any style by effectively merging loras. In *European Conference on Computer Vision*, pages 422–438. Springer, 2025. 2, 3, 4, 6, 7, 15
- [50] Chongjie Si, Zhiyi Shi, Shifan Zhang, Xiaokang Yang, Hanspeter Pfister, and Wei Shen. Unleashing the power of task-specific directions in parameter efficient fine-tuning. In *The Thirteenth International Conference on Learning Representations*, 2025. 2
- [51] Enis Simsar, Thomas Hofmann, Federico Tombari, and Pinar Yanardag. Loraclr: Contrastive adaptation for customization of diffusion models. *CVPR*, 2025. 3
- [52] Kihyuk Sohn, Lu Jiang, Jarred Barber, Kimin Lee, Nataniel Ruiz, Dilip Krishnan, Huiwen Chang, Yuanzhen Li, Irfan Essa, Michael Rubinstein, et al. Styledrop: Text-to-image synthesis of any style. *Advances in Neural Information Processing Systems*, 36, 2024. 2, 3, 6
- [53] Jiaming Song, Chenlin Meng, and Stefano Ermon. Denoising diffusion implicit models. In *ICLR*, 2021. 1, 2
- [54] Yang Song, Jascha Sohl-Dickstein, Diederik P Kingma, Abhishek Kumar, Stefano Ermon, and Ben Poole. Score-based generative modeling through stochastic differential equations. In *ICLR*, 2021. 1, 2, 3
- [55] Yi-Lin Sung, Jaemin Cho, and Mohit Bansal. V1-adapter: Parameter-efficient transfer learning for vision-and-language

- tasks. In *Proceedings of the IEEE/CVF conference on computer vision and pattern recognition*, pages 5227–5237, 2022. 2
- [56] Genmo Team. Mochi 1. <https://github.com/genmoai/models>, 2024. 9
- [57] Chunlin Tian, Zhan Shi, Zhijiang Guo, Li Li, and Chengzhong Xu. Hydralora: An asymmetric lora architecture for efficient fine-tuning. In *Advances in Neural Information Processing Systems (NeurIPS)*, 2024. 2
- [58] Narek Tumanyan, Michal Geyer, Shai Bagon, and Tali Dekel. Plug-and-play diffusion features for text-driven image-to-image translation. In *Proceedings of the IEEE/CVF Conference on Computer Vision and Pattern Recognition*, pages 1921–1930, 2023. 3
- [59] A Vaswani. Attention is all you need. *Advances in Neural Information Processing Systems*, 2017. 3
- [60] Patrick von Platen, Suraj Patil, Anton Lozhkov, Pedro Cuenca, Nathan Lambert, Kashif Rasul, Mishig Davaadorj, Dhruv Nair, Sayak Paul, William Berman, Yiyi Xu, Steven Liu, and Thomas Wolf. Diffusers: State-of-the-art diffusion models. <https://github.com/huggingface/diffusers>, 2022. 6, 7
- [61] Haofan Wang, Qixun Wang, Xu Bai, Zekui Qin, and Anthony Chen. Instantstyle: Free lunch towards style-preserving in text-to-image generation. *arXiv preprint arXiv:2404.02733*, 2024. 2, 3
- [62] Qiucheng Wu, Yujian Liu, Handong Zhao, Ajinkya Kale, Trung Bui, Tong Yu, Zhe Lin, Yang Zhang, and Shiyu Chang. Uncovering the disentanglement capability in text-to-image diffusion models. In *Proceedings of the IEEE/CVF conference on computer vision and pattern recognition*, pages 1900–1910, 2023. 3
- [63] Guangxuan Xiao, Tianwei Yin, William T. Freeman, Frédo Durand, and Song Han. Fastcomposer: Tuning-free multi-subject image generation with localized attention. *International Journal of Computer Vision*, 2024. 3
- [64] Lingling Xu, Haoran Xie, Si-Zhao Joe Qin, Xiaohui Tao, and Fu Lee Wang. Parameter-efficient fine-tuning methods for pretrained language models: A critical review and assessment. *arXiv preprint arXiv:2312.12148*, 2023. 2
- [65] Alice Xue. End-to-end chinese landscape painting creation using generative adversarial networks. In *Proceedings of the IEEE/CVF Winter conference on applications of computer vision*, pages 3863–3871, 2021. 6
- [66] Jiahui Yang, Donglin Di, Baorui Ma, Xun Yang, Yongjia Ma, Wenzhang Sun, Wei Chen, Jianxun Cui, Zhou Xue, Meng Wang, et al. Tv-3dg: Mastering text-to-3d customized generation with visual prompt. *arXiv preprint arXiv:2410.21299*, 2024. 9
- [67] Serin Yang, Hyunmin Hwang, and Jong Chul Ye. Zero-shot contrastive loss for text-guided diffusion image style transfer. In *Proceedings of the IEEE/CVF International Conference on Computer Vision*, pages 22873–22882, 2023. 3
- [68] Xun Yang, Fuli Feng, Wei Ji, Meng Wang, and Tat-Seng Chua. Deconfounded video moment retrieval with causal intervention. In *Proceedings of the 44th International ACM SIGIR Conference on Research and Development in Information Retrieval*, page 1–10, New York, NY, USA, 2021. Association for Computing Machinery. 2
- [69] Xun Yang, Shanshan Wang, Jian Dong, Jianfeng Dong, Meng Wang, and Tat-Seng Chua. Video moment retrieval with cross-modal neural architecture search. *IEEE Transactions on Image Processing*, 31:1204–1216, 2022. 9
- [70] Xun Yang, Jianming Zeng, Dan Guo, Shanshan Wang, Jianfeng Dong, and Meng Wang. Robust video question answering via contrastive cross-modality representation learning. *Science China Information Sciences*, 67(10):202104, 2024.
- [71] Zhuoyi Yang, Jiayan Teng, Wendi Zheng, Ming Ding, Shiyu Huang, Jiazheng Xu, Yuanming Yang, Wenyi Hong, Xiaohan Zhang, Guanyu Feng, et al. Cogvideox: Text-to-video diffusion models with an expert transformer. *arXiv preprint arXiv:2408.06072*, 2024. 9
- [72] Hu Ye, Jun Zhang, Sibio Liu, Xiao Han, and Wei Yang. Ip-adapt: Text compatible image prompt adapter for text-to-image diffusion models. *arXiv preprint arXiv:2308.06721*, 2023. 1, 2, 3
- [73] Lvmin Zhang, Anyi Rao, and Maneesh Agrawala. Adding conditional control to text-to-image diffusion models. In *ICCV*, pages 3836–3847, 2023. 1, 2, 3
- [74] Ming Zhong, Yelong Shen, Shuohang Wang, Yadong Lu, Yizhu Jiao, Siru Ouyang, Donghan Yu, Jiawei Han, and Weizhu Chen. Multi-lora composition for image generation. *arXiv preprint arXiv:2402.16843*, 2024. 2, 4
- [75] Sheng Zhou, Junbin Xiao, Qingyun Li, Yicong Li, Xun Yang, Dan Guo, Meng Wang, Tat-Seng Chua, and Angela Yao. Egotextvqa: Towards egocentric scene-text aware video question answering. In *Proceedings of the Computer Vision and Pattern Recognition Conference (CVPR)*, pages 3363–3373, 2025. 9
- [76] Xiandong Zou, Mingzhu Shen, Christos-Savvas Bouganis, and Yiren Zhao. Cached multi-lora composition for multi-concept image generation. In *ICLR*, 2025. 2, 4

Appendix of QR-LoRA: Efficient and Disentangled Fine-tuning via QR Decomposition for Customized Generation

(Supplementary Material)

A. Theoretical Analysis of QR-LoRA Parameter Disentanglement

A.1. Minimal Frobenius Norm Property

Lemma 1 (Minimal Frobenius Norm Property of QR-LoRA Parameterization). *Consider a weight matrix $W \in \mathbb{R}^{m \times n}$ with a low-rank update $\Delta W = Q\Delta R$, where $Q \in \mathbb{R}^{m \times r}$ is a column-orthogonal matrix (i.e., $Q^\top Q = I_r$), and $\Delta R \in \mathbb{R}^{r \times n}$ represents trainable parameters. For any rank- r update ΔW , the parameterization $\Delta W = Q\Delta R$ achieves the minimal Frobenius norm if and only if Q is column-orthogonal, yielding:*

$$\|\Delta W\|_F = \|Q\Delta R\|_F = \|\Delta R\|_F, \quad (8)$$

with ΔR having a unique solution under orthogonal constraints.

Proof. Leveraging the norm-preserving property of orthogonal matrices, for any column-orthogonal Q , we have:

$$\begin{aligned} \|Q\Delta R\|_F &= \sqrt{\text{tr}(\Delta R^\top Q^\top Q \Delta R)} \\ &= \sqrt{\text{tr}(\Delta R^\top \Delta R)} \\ &= \|\Delta R\|_F, \end{aligned} \quad (9)$$

consequently, the Frobenius norm of the parameterized update $\Delta W = Q\Delta R$ is equivalent to the norm of ΔR . \square

This equivalence has profound implications for our framework:

- **Minimal Intervention Principle:** The uniqueness of the minimal norm solution reflects the optimal task-specific transformation. For any target weight update ΔW , we seek its representation in the form of $Q\Delta R$, where Q is column-orthogonal. Among multiple solutions satisfying the task objective, the minimal norm solution maximally preserves the model’s original generalization capabilities while introducing only necessary task-specific transformations.
- **Task-Specific Feature Encoding:** The minimal norm property of ΔR prevents overfitting by incorporating only the minimal changes required for the specific task. This principle ensures that ΔR exclusively encodes information relevant to the current task, avoiding the incorporation of general features shared across different tasks.

A.2. Gradient Update Decoupling Analysis

Theorem 1 (Statistical Independence of Orthogonal Projections). *In a Hilbert space with orthogonal basis, projections along different feature directions are statistically independent. Specifically, for any two orthogonal directions v_i and v_j ($v_i^\top v_j = 0$), the projections of a random vector x onto these directions, denoted as $P_i(x)$ and $P_j(x)$ respectively, are statistically uncorrelated:*

$$E[P_i(x)P_j(x)] = 0, \quad (10)$$

where $E[\cdot]$ denotes the expectation operator.

In the context of Hilbert spaces with orthogonal bases, projections along different feature directions exhibit statistical independence. This fundamental property plays a crucial role in our QR-LoRA framework, where the Q matrix defines a set of orthogonal basis vectors, and the ΔR matrix represents coordinates in this orthogonal basis system. The gradient update mechanism in our framework demonstrates how this orthogonality naturally leads to feature disentanglement. For a loss function $\mathcal{L}(W)$ with the parameterization $W = W_{\text{comp}} + Q(R + \Delta R)$, the gradient update mechanism exhibits the following key property:

The gradient of the loss with respect to ΔR is given by:

$$\frac{\partial \mathcal{L}}{\partial \Delta R} = \frac{\partial \mathcal{L}}{\partial W} \cdot \frac{\partial W}{\partial \Delta R} = Q^\top \frac{\partial \mathcal{L}}{\partial W}. \quad (11)$$

Given the column orthogonality of Q ($Q^\top Q = I$), this gradient formulation reveals that $\partial \mathcal{L} / \partial \Delta R$ is an orthogonal projection of $\partial \mathcal{L} / \partial W$ onto the column space of Q . This projection mechanism is particularly significant when training for different tasks (e.g., style or content adaptation), as these tasks inherently optimize distinct visual attributes. The orthogonality of their gradient directions in the high-dimensional space is preserved and enhanced through the Q matrix projection, causing different ΔR matrices to evolve along approximately orthogonal trajectories during training.

To provide a comprehensive understanding of QR-LoRA’s theoretical advantages, we further analyze its forward pass and gradient computation mechanisms in comparison with existing methods. Table 2 presents a detailed comparison of the forward pass and gradient computation between QR-LoRA and other representative approaches.

As shown in Table 2, QR-LoRA fundamentally differs from previous approaches in both its forward pass computation and gradient update mechanism. While traditional LoRA [17] and Ortha [43] rely on random initialization and

Table 2. **Summary of forward pass and gradient computation in different methods.** This comparison highlights QR-LoRA’s unique orthogonal projection-based gradient update mechanism, which naturally leads to more effective feature disentanglement compared to traditional approaches.

	LoRA [17]	Ortha [43]	QR-LoRA
Forward	$Y = X(W + BA)$ $A \sim \mathcal{N}(0, \sigma^2) \in \mathbb{R}^{r \times n}$ $B = 0 \in \mathbb{R}^{m \times r}$	$Y = X(W + BA)$ $A \sim \mathcal{N}(0, \sigma^2) \in \mathbb{R}^{r \times n}$ $B \sim \mathcal{N}(0, \sigma^2) \in \mathbb{R}^{m \times r}$	$Y = XW; W = U\Sigma V^\top$ $W_{core}^\top = V_{[:,r]} \Sigma_{[r]} U_{[:,r]}^\top = QR$ $W = W_{comp} + (Q(R + \Delta R))^\top$
Gradient	$\frac{\partial \mathcal{L}}{\partial A} = B^\top \frac{\partial \mathcal{L}}{\partial W} \Rightarrow \mathbf{0}$ $\frac{\partial \mathcal{L}}{\partial B} = \frac{\partial \mathcal{L}}{\partial W} A^\top \Rightarrow \mathbf{Random}$	frozen B , train A $\frac{\partial \mathcal{L}}{\partial A} = B^\top \frac{\partial \mathcal{L}}{\partial W} \Rightarrow \mathbf{Random}$	$Q \in \mathbb{R}^{n \times r}, R \in \mathbb{R}^{r \times m}$; train ΔR $\frac{\partial \mathcal{L}}{\partial \Delta R} = Q^\top \frac{\partial \mathcal{L}}{\partial W} \Rightarrow \mathbf{Primary}$

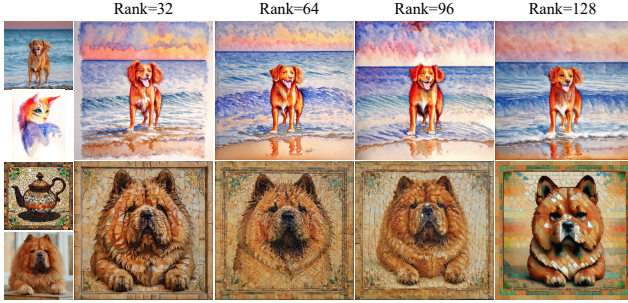


Figure 10. **Rank sensitivity analysis.** Our method maintains stable performance across different rank settings, demonstrating its robustness to this hyperparameter choice.

direct parameter updates, our method leverages orthogonal decomposition to achieve more principled and effective parameter updates.

A.3. Theoretical Interpretation of Experimental Observations

- **Stability of Q :** The stability of Q matrices across different tasks stems from their construction through SVD-based QR decomposition, where their directions are primarily determined by the underlying data distribution, leading to consistently high similarities.
- **Independence of ΔR :** The orthogonal projection property ensures that ΔR matrices exclusively capture task-specific information, resulting in significant variations that reflect the unique characteristics of different tasks.

B. Additional Implementation Details

B.1. Implementation Details of Compared Methods.

In our comprehensive evaluation, we implement ZipLoRA based on an unofficial implementation¹, configuring it with rank $r = 64$ and learning rate $5e-5$. For StyleAligned and

¹<https://github.com/mkshing/ziploara-pytorch>

B-LoRA, we adopt their respective default configurations from the original papers. Additionally, we employ the standard DreamBooth-LoRA implementation for experiments on SD3 and FLUX.1-dev models, maintaining consistent hyperparameters ($r = 64$, $lr=1e-4$) across all comparisons to ensure fairness.

Model-specific Training Configurations. Across all backbone models, we exclusively inject QR-LoRA modules into the main generative networks (*e.g.*, UNet, MM-DiT) while keeping the text encoders frozen during training. For different backbone models, we inject QR-LoRA modules into specific layers as shown in Table 3:

- **SDXL:** We inject our QR-LoRA modules into the self-attention layers of UNet only, focusing on the core architecture components. For inference, we use 50 denoising steps while keeping other parameters at their default values.
- **SD3:** Following the model architecture, we apply our method to both standard attention blocks and additional projection layers unique to SD3. During inference, we employ 28 denoising steps with default configurations for other parameters.
- **FLUX.1-dev:** We extend the injection to include both attention mechanisms and feedforward networks, covering the expanded architecture of FLUX.1-dev. Similar to SD3, we use 28 denoising steps for inference while maintaining default settings for other parameters.

C. Additional Analysis Details and Results

C.1. Experimental Setup for Matrix Similarity Analysis

To comprehensively evaluate the feature disentanglement capabilities of our QR-LoRA framework, we conduct extensive experiments using 27 randomly selected image pairs (sample index from 0-26), as visualized in Figure 13. For each image pair, we analyze three different training strategies: (1) a QR decomposition variant where both Q and

Table 3. **Injection layer types of QR-LoRA across different backbone models.** This table details the specific architectural components where our QR-LoRA modules are injected during training across different foundation models (SDXL, SD3, and FLUX.1-dev), demonstrating the practical implementation of our method’s disentangled fine-tuning approach.

SDXL	SD3	FLUX.1-dev
to_k	attn.to_k	attn.to_k
to_q	attn.to_q	attn.to_q
to_v	attn.to_v	attn.to_v
to_out.0	attn.to_out.0	attn.to_out.0
	attn.add_k_proj	attn.add_k_proj
	attn.add_q_proj	attn.add_q_proj
	attn.add_v_proj	attn.add_v_proj
	attn.to_add_out	attn.to_add_out
		ff.net.0.proj
		ff.net.2
		ff_context.net.0.proj
		ff_context.net.2

R matrices are directly fine-tuned, (2) a ΔR -only update strategy, and (3) vanilla LoRA with A and B matrices. The cosine similarities between corresponding matrices across different training instances are computed and recorded in Table 4, with their distributions visualized in Figure 2 of the main text. This experimental design allows us to analyze the inherent properties of different matrices and their roles in feature representation.

C.2. Cross-Model Analysis of Matrix Properties

We extend our analysis across three state-of-the-art text-to-image models: SDXL, SD3, and FLUX.1-dev, to validate the model-agnostic nature of our approach. As shown in Figure 14, Figure 16, and Figure 15, the layer-wise cosine similarity patterns remain consistent across different model architectures, demonstrating the generalizability of our QR-LoRA framework. Specifically:

- **Q Matrix Properties:** Across all models, Q matrices maintain remarkably high similarities (0.90-0.99), indicating their role as stable orthogonal bases for feature representation.
- **R Matrix Characteristics:** The directly fine-tuned R matrices show moderate but significant similarities (0.79-0.89), suggesting their inherited structural information from the original weights.
- **ΔR Matrix Behavior:** In contrast, ΔR matrices consistently exhibit substantially lower similarities (-0.17-0.25), validating their effectiveness in capturing task-specific features independently.

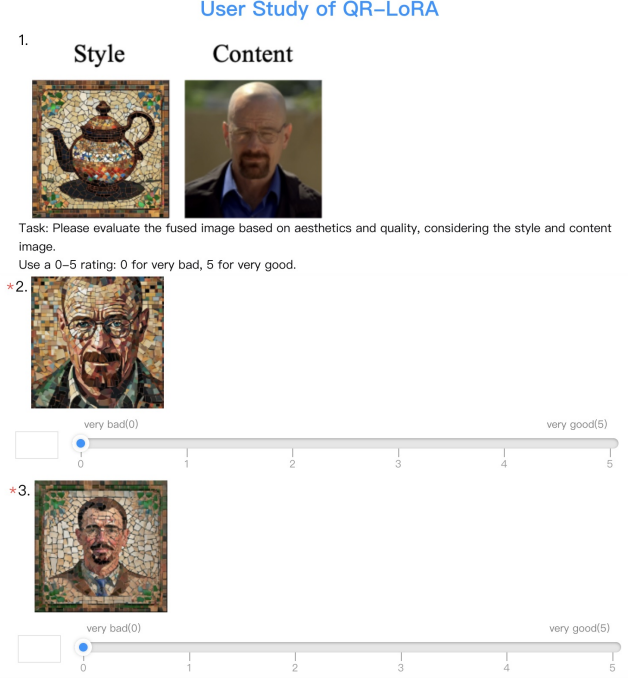


Figure 11. **User study interface.** Screenshot of our evaluation interface where participants rate generated images on a 0-5 scale based on content preservation and style transfer quality.

C.3. Statistical Analysis of Matrix Similarities

The numerical results presented in Table 4 provide a detailed quantitative perspective on the similarity patterns. The data reveals several key insights:

- The maximum similarity values for Q matrices consistently approach 1.0 (0.9998-0.9999), with minimum values remaining above 0.90, demonstrating the stability of the orthogonal basis.
- R matrices show maximum similarities above 0.99 but with lower minimum values (0.79-0.89), reflecting their role in capturing task-relevant transformations while maintaining some degree of shared structure.
- ΔR matrices exhibit significantly lower similarity values, with maximums below 0.26 and minimums reaching -0.17, quantitatively confirming their capacity for independent feature representation.
- In comparison, traditional LoRA’s A matrices show consistently high similarities (0.77-1.0), while B matrices display moderate to low similarities (0.15-0.38), highlighting the advantages of our orthogonal decomposition approach.

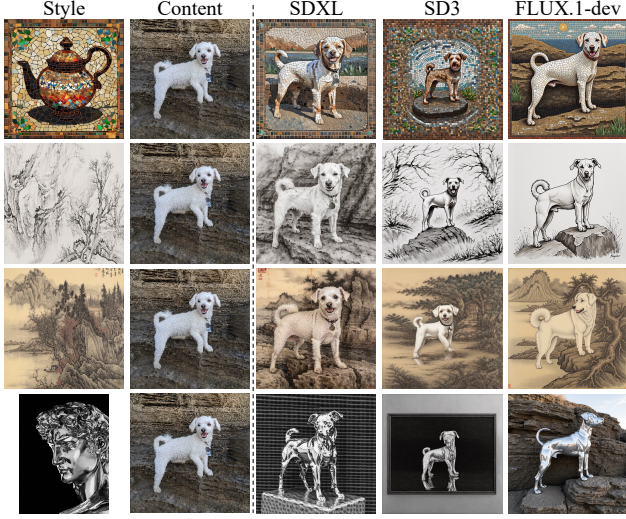


Figure 12. **Additional visualization results on different backbone models.** Extended demonstration of QR-LoRA’s generation results across SDXL, SD3, and FLUX.1-dev models, further validating the consistent high-quality performance and model-agnostic nature of our approach. These supplementary examples provide a more comprehensive view of our method’s capabilities across diverse model architectures, complementing the results presented in Figure 6.

This comprehensive analysis validates the theoretical foundations of our QR-LoRA framework and demonstrates its effectiveness in achieving feature disentanglement across different model architectures. The consistent patterns observed in both layer-wise visualizations and statistical distributions support our design choice of focusing on ΔR updates for efficient and clean feature separation.

D. Additional Experimental Results and Discussion

D.1. Ablation Studies

Scaling coefficient. To comprehensively evaluate the robustness and flexibility of our QR-LoRA framework, we conduct extensive ablation studies on scaling coefficients across three different backbone models: SDXL, SD3, and FLUX.1-dev. Our experiments systematically explore coefficient combinations (*i.e.*, λ_c , λ_s) ranging from 0.5 to 1.0 with intervals of 0.1, resulting in 36 distinct combinations for each model. This granular analysis reveals several key insights about our method’s behavior and capabilities.

As demonstrated in Figures 17, 18, and 19, our approach maintains consistent generation quality across different coefficient settings while enabling fine-grained control over the content-style fusion process. The smooth transitions observed between different coefficient combinations indicate that our QR decomposition effectively disentangles content

and style features, allowing for intuitive and stable interpolation between these attributes. Notably, this behavior remains consistent across all three model architectures, validating the model-agnostic nature of our approach.

Furthermore, our experiments demonstrate that our method exhibits robust performance across a wide range of scaling coefficients after obtaining the disentangled ΔR matrices. This scaling exploration serves as a deeper investigation into our method’s capabilities, rather than a limitation. It’s worth noting that such scaling strategies are generally applicable to any LoRA-based methods, showcasing the versatility of our approach in achieving various levels of content preservation and style transfer effects.

Rank. To comprehensively evaluate the robustness of our method, we conduct a sensitivity analysis across different rank settings. As shown in Figure 10, our method demonstrates consistent performance and stable generation quality across various rank values, indicating its inherent robustness to this hyperparameter. We adopt rank=64 for all experiments in the main paper, as it strikes an optimal balance between computational efficiency and generation quality. This choice aligns well with common practices in the literature [8, 49] and proves to be a reliable setting for most applications.

D.2. User Study

To evaluate the perceptual quality of our results, we conducted a comprehensive user study with 47 participants (40 males and 7 females). The participants represented a diverse demographic, with ages ranging from 22 to 45 years (mean age: 31.2). Among the participants, 15 were computer vision researchers, 12 were professional designers, and 20 were general users with basic knowledge of image editing. This diverse composition ensured a balanced evaluation from both technical and aesthetic perspectives.

Each participant was asked to rate the quality of generated images from different methods on a scale of 0-5, where 0 indicates poor quality and 5 indicates excellent quality. To facilitate the evaluation process, we designed an intuitive rating interface (shown in Figure 11) that allows participants to easily assess and score the generated images. The evaluation criteria focused on both content preservation and style transfer aspects. The ratings reported in Table 1 represent the average scores given by participants for each method. The consistently higher ratings achieved by our method (4.07 for SDXL, 4.14 for SD3, and 3.96 for FLUX.1-dev) compared to baseline approaches demonstrate the superior perceptual quality across different backbone models.

D.3. Additional Qualitative Results

To comprehensively demonstrate the effectiveness and versatility of our QR-LoRA framework, we present extensive

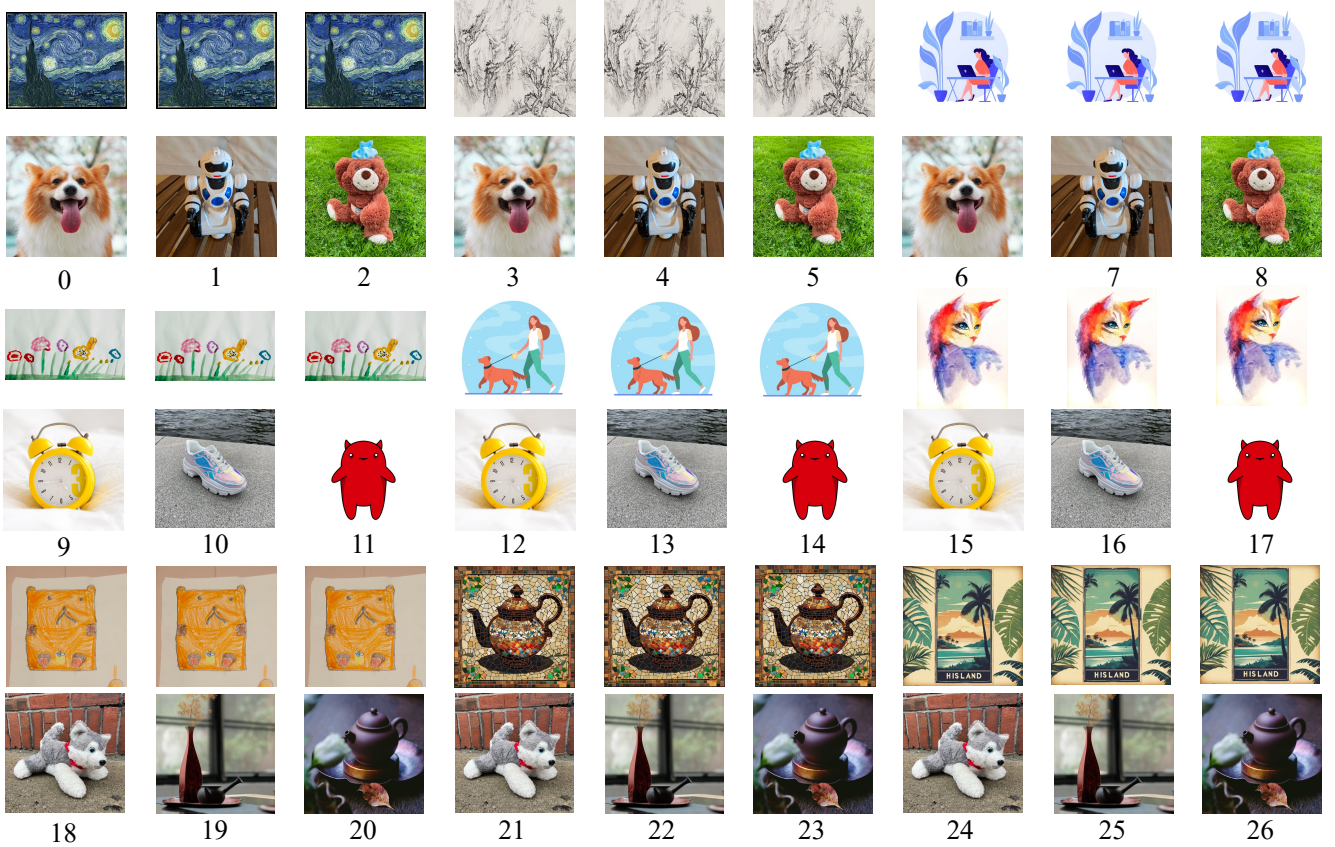


Figure 13. **Detailed experimental setup for matrix similarity comparison in Figure 2.** We conduct experiments on 27 randomly selected image pairs to analyze the properties of different matrices in our QR-LoRA framework. For each image in the pairs, we train two types of LoRA adaptations: one using QR decomposition where both Q and R matrices are directly fine-tuned and another using the ΔR formulation. We then compute the cosine similarities between Q matrices, R matrices, and ΔR matrices across all injection layers in the SDXL model.

qualitative results across different backbone models and diverse application scenarios. First, we conduct a thorough comparative analysis through Figure 20, which showcases our method’s superior performance against state-of-the-art approaches across SDXL, SD3, and FLUX.1-dev models. The results consistently demonstrate QR-LoRA’s ability to achieve better content preservation while maintaining high-fidelity style transfer, regardless of the underlying model architecture.

To further validate the model-agnostic nature of our approach, we present a comprehensive set of generation results across different backbone architectures. Figures 21, 22, and 23 showcase diverse generation results on SDXL, demonstrating our method’s capability in handling various challenging scenarios while maintaining high visual quality and style fidelity. The results span a wide range of content types and artistic styles, from intricate architectural details to subtle texture variations.

Extending our analysis to other backbone architectures,

Figure 24 presents generation results on SD3, while Figure 25 shows results using FLUX.1-dev as the backbone. These examples demonstrate that QR-LoRA maintains its effectiveness across different model architectures, consistently producing high-quality results that effectively balance content preservation and style transfer.

Collectively, these results validate the robustness and generalization capability of our approach across diverse scenarios. The consistent high-quality performance across different content types (*e.g.*, portraits, objects) and artistic styles (*e.g.*, watercolor, digital art) demonstrates QR-LoRA’s effectiveness in handling complex geometric structures, fine-grained textures, and dramatic style variations. This comprehensive evaluation further supports the model-agnostic nature of our method and its potential for broad application in various image generation and style transfer tasks.

Table 4. **Numerical results of matrix similarity comparison in Figure 2.** This table presents the detailed cosine similarity values for Q matrices, R matrices, ΔR matrices, A matrices, and B matrices from 27 pairs of image training data. For each image pair (*i.e.*, sample index), we compute the cosine similarities across all injection layers in the SDXL model and record both the maximum (Q_{max} , R_{max} , ΔR_{max} , A_{max} , B_{max}) and minimum (Q_{min} , R_{min} , ΔR_{min} , A_{min} , B_{min}) similarity values.

Sample Index	Q_{max}	Q_{min}	R_{max}	R_{min}	ΔR_{max}	ΔR_{min}	A_{max}	A_{min}	B_{max}	B_{min}
0	0.9999	0.9787	0.9997	0.8409	0.1657	-0.1139	1.0000	0.8046	0.3615	-0.0355
1	0.9999	0.9786	0.9997	0.8253	0.1632	-0.1223	1.0000	0.7970	0.3249	-0.0625
2	0.9999	0.9682	0.9997	0.8391	0.1135	-0.1038	1.0000	0.8161	0.3198	-0.0826
3	0.9998	0.9311	0.9996	0.8104	0.1959	-0.1335	1.0000	0.8075	0.2322	-0.0565
4	0.9998	0.9313	0.9996	0.7993	0.1241	-0.0818	1.0000	0.8020	0.2295	-0.0626
5	0.9998	0.9055	0.9997	0.8143	0.1529	-0.0872	1.0000	0.8144	0.2226	-0.0558
6	0.9998	0.9679	0.9997	0.8235	0.1566	-0.0581	1.0000	0.7917	0.2113	-0.0807
7	0.9999	0.9680	0.9997	0.8129	0.1421	-0.0699	1.0000	0.8126	0.2145	-0.0783
8	0.9999	0.9761	0.9997	0.8187	0.1257	-0.0913	1.0000	0.8053	0.1898	-0.2033
9	0.9999	0.9709	0.9998	0.8441	0.1749	-0.1036	1.0000	0.8272	0.3044	-0.1188
10	0.9999	0.9741	0.9998	0.8245	0.1500	-0.0783	1.0000	0.8163	0.2070	-0.0793
11	0.9999	0.9792	0.9998	0.8833	0.1399	-0.0611	1.0000	0.8379	0.1525	-0.1278
12	0.9999	0.9765	0.9997	0.8485	0.1816	-0.1094	1.0000	0.8253	0.2499	-0.0961
13	0.9999	0.9793	0.9998	0.8216	0.2493	-0.0463	1.0000	0.8164	0.1490	-0.1374
14	0.9999	0.9854	0.9999	0.8894	0.2067	-0.0933	1.0000	0.8332	0.1817	-0.1316
15	0.9998	0.9724	0.9996	0.8410	0.1756	-0.1686	1.0000	0.8416	0.3820	-0.0801
16	0.9998	0.9752	0.9996	0.8186	0.1851	-0.1050	1.0000	0.8361	0.2329	-0.0636
17	0.9998	0.9807	0.9997	0.8818	0.1262	-0.0695	1.0000	0.8413	0.2125	-0.1462
18	0.9999	0.9055	0.9996	0.8340	0.2539	-0.0760	1.0000	0.8346	0.3847	-0.2045
19	0.9999	0.9054	0.9997	0.8408	0.1209	-0.0420	1.0000	0.8398	0.2905	-0.0762
20	0.9999	0.9053	0.9996	0.8339	0.1705	-0.0540	1.0000	0.8298	0.2734	-0.0548
21	0.9998	0.9045	0.9995	0.8040	0.2042	-0.0466	1.0000	0.7727	0.1746	-0.0739
22	0.9998	0.9044	0.9995	0.8095	0.1441	-0.0716	1.0000	0.7714	0.1531	-0.1031
23	0.9998	0.9045	0.9995	0.7992	0.1473	-0.0588	1.0000	0.7853	0.1558	-0.0861
24	0.9998	0.9055	0.9996	0.8272	0.1711	-0.0512	1.0000	0.8034	0.1969	-0.0806
25	0.9998	0.9053	0.9996	0.8207	0.1686	-0.0851	1.0000	0.8147	0.2685	-0.0401
26	0.9998	0.9053	0.9996	0.8134	0.1719	-0.0850	1.0000	0.8108	0.2691	-0.0488

D.4. Ability to Re-contextualize

Our method not only excels at fusing content and style but also enables further customization through text prompts. While maintaining the high-quality integration of content and style elements, our approach supports flexible scene manipulation through additional textual instructions, as shown in Figure 26. For instance, given a content image of a dog and a specific artistic style, we can generate variations like "wearing a hat" or "riding a bicycle" while preserving the desired style characteristics. This re-contextualization capability is particularly valuable in practical artistic applications, as it allows artists to explore diverse creative possibilities while maintaining consistent stylistic elements across different scenarios.

sion tasks requiring robust disentanglement properties, such as the fusion of arbitrary style and content. This stands in contrast to the field’s ongoing trend of pursuing specific disentanglement properties within particular models.

D.5. The End

We anticipate that our model-agnostic, low-rank efficient fine-tuning approach will provide a versatile solution for fu-

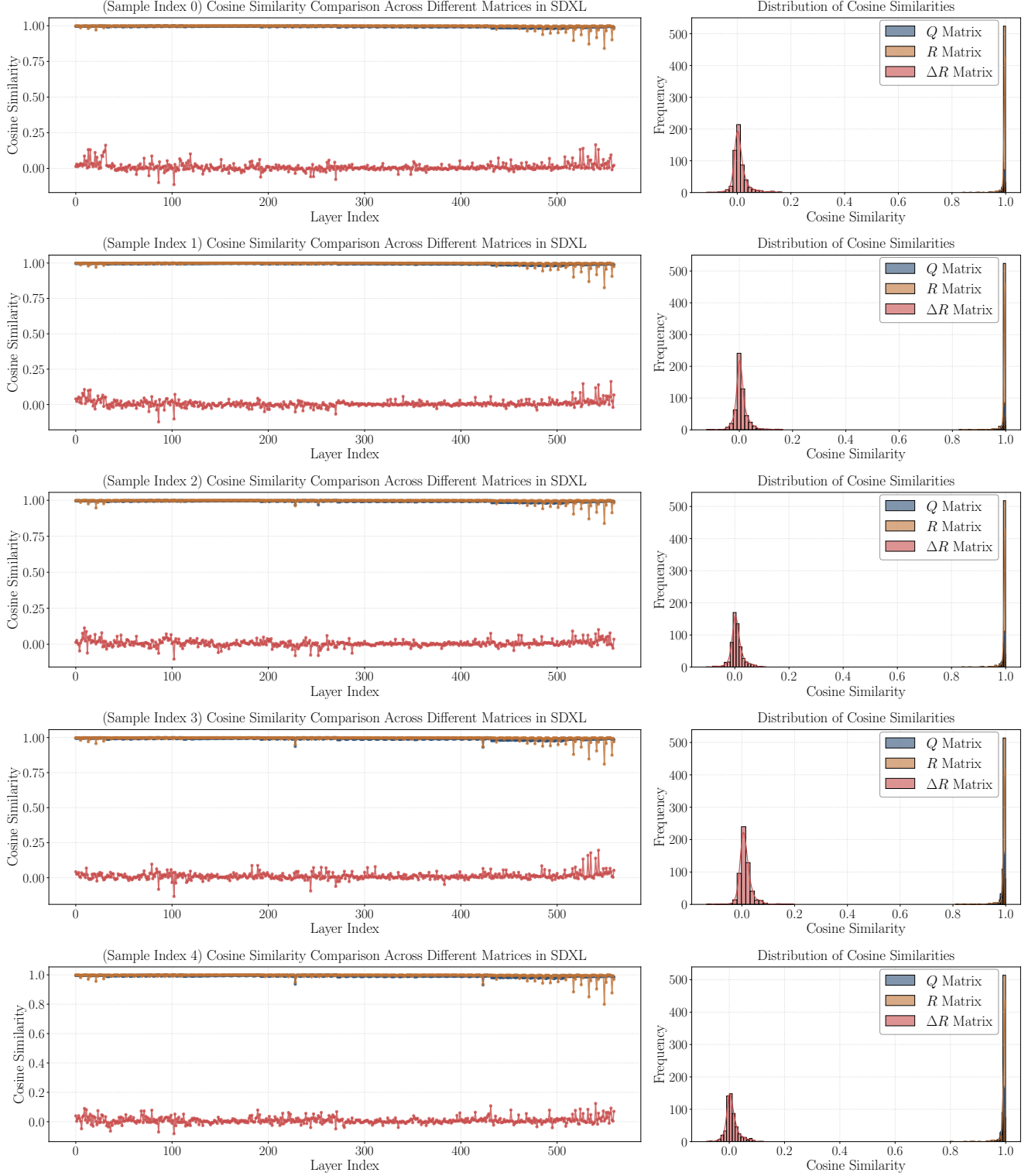


Figure 14. **Extended analysis of cosine similarities under SDXL model, complementing Figure 3.** We replicate the similarity analysis experiment (sample index from 0 to 4) from Figure 3 using the SDXL backbone model to validate the generalization of our findings. The left panel shows the layer-wise cosine similarity trends across different training strategies, consistent with our main results. Additionally, we provide histogram distributions of similarity values in the right panel, offering a statistical perspective on the similarity patterns. This comprehensive visualization further supports our theoretical analysis by demonstrating that the observed matrix properties are consistent across different model architectures.

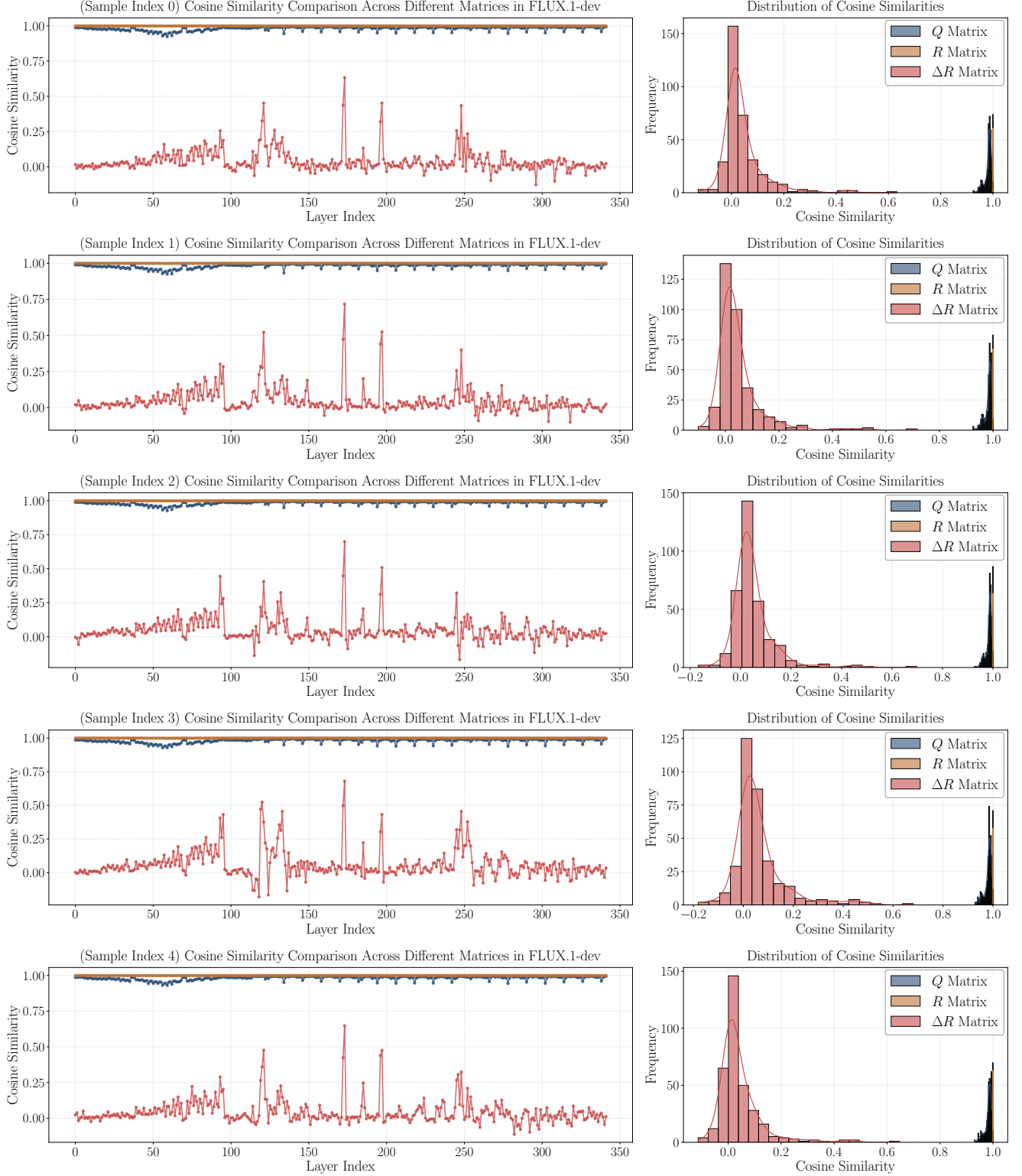


Figure 15. **Extended analysis of cosine similarities under FLUX.1-dev model, complementing Figure 3.** We replicate the similarity analysis experiment (sample index from 0 to 4) from Figure 3 using the FLUX.1-dev backbone model to validate the generalization of our findings. The left panel shows the layer-wise cosine similarity trends across different training strategies, consistent with our main results. Additionally, we provide histogram distributions of similarity values in the right panel, offering a statistical perspective on the similarity patterns. This comprehensive visualization further supports our theoretical analysis by demonstrating that the observed matrix properties are consistent across different model architectures.

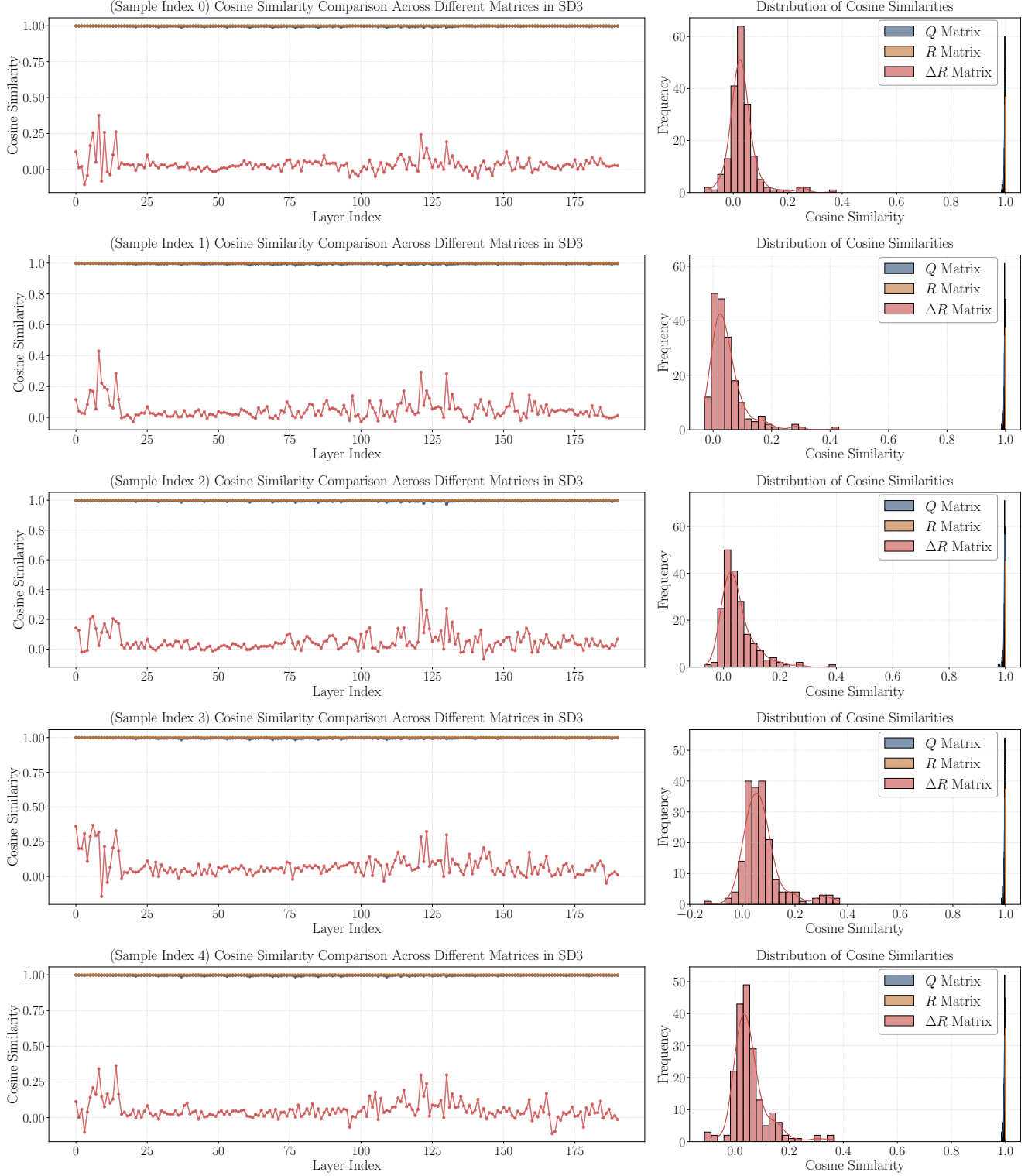


Figure 16. **Extended analysis of cosine similarities under SD3 model, complementing Figure 3.** We replicate the similarity analysis experiment (sample index from 0 to 4) from Figure 3 using the SD3 backbone model to validate the generalization of our findings. The left panel shows the layer-wise cosine similarity trends across different training strategies, consistent with our main results. Additionally, we provide histogram distributions of similarity values in the right panel, offering a statistical perspective on the similarity patterns. This comprehensive visualization further supports our theoretical analysis by demonstrating that the observed matrix properties are consistent across different model architectures.

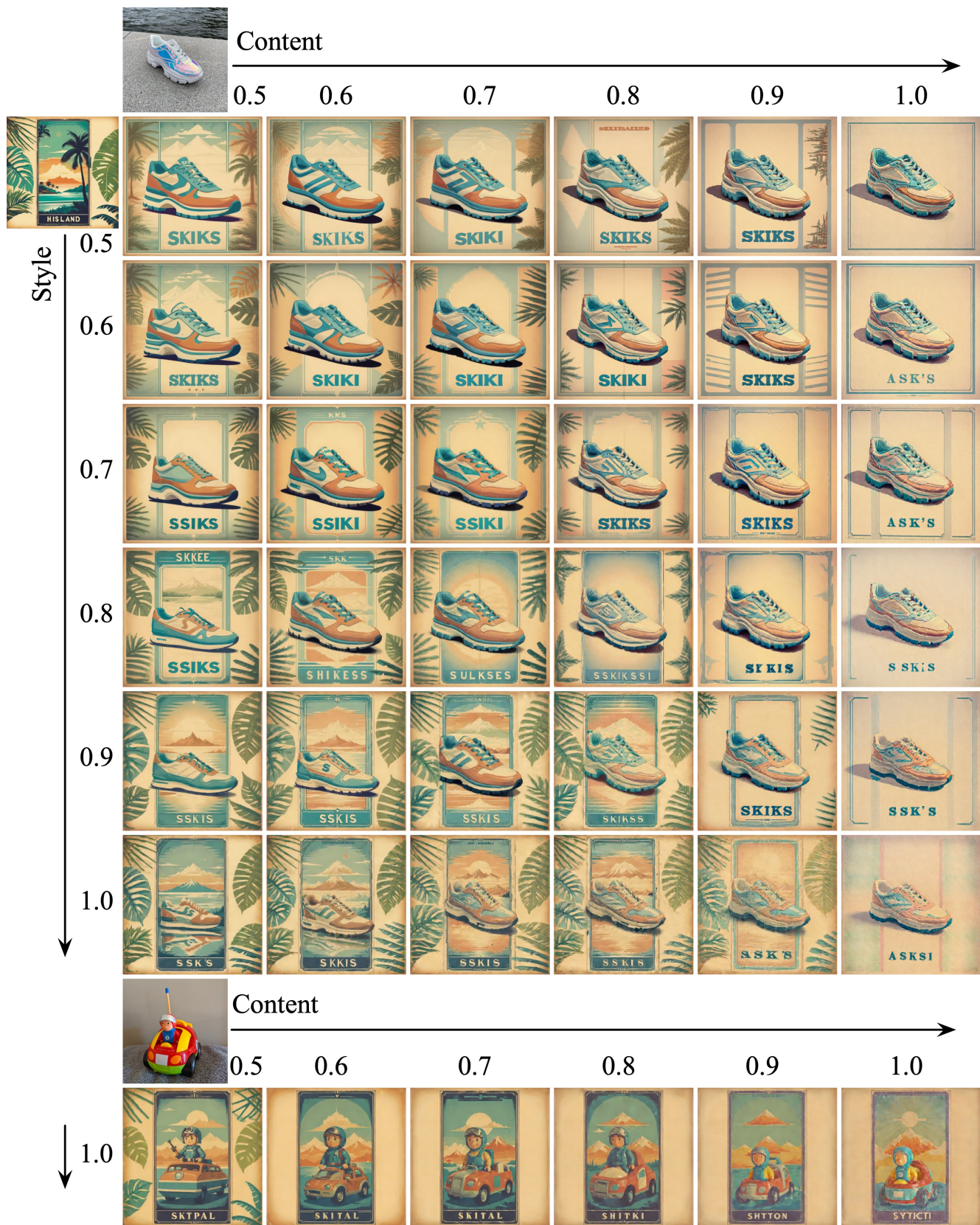


Figure 17. **Comprehensive ablation study on scaling coefficients for content-style fusion based on SDXL.** We demonstrate the generation results under various combinations of content and style scaling coefficients. The experiments validate the flexibility and robustness of our approach in achieving fine-grained control over content-style fusion through different coefficient combinations. Please zoom in to view details.

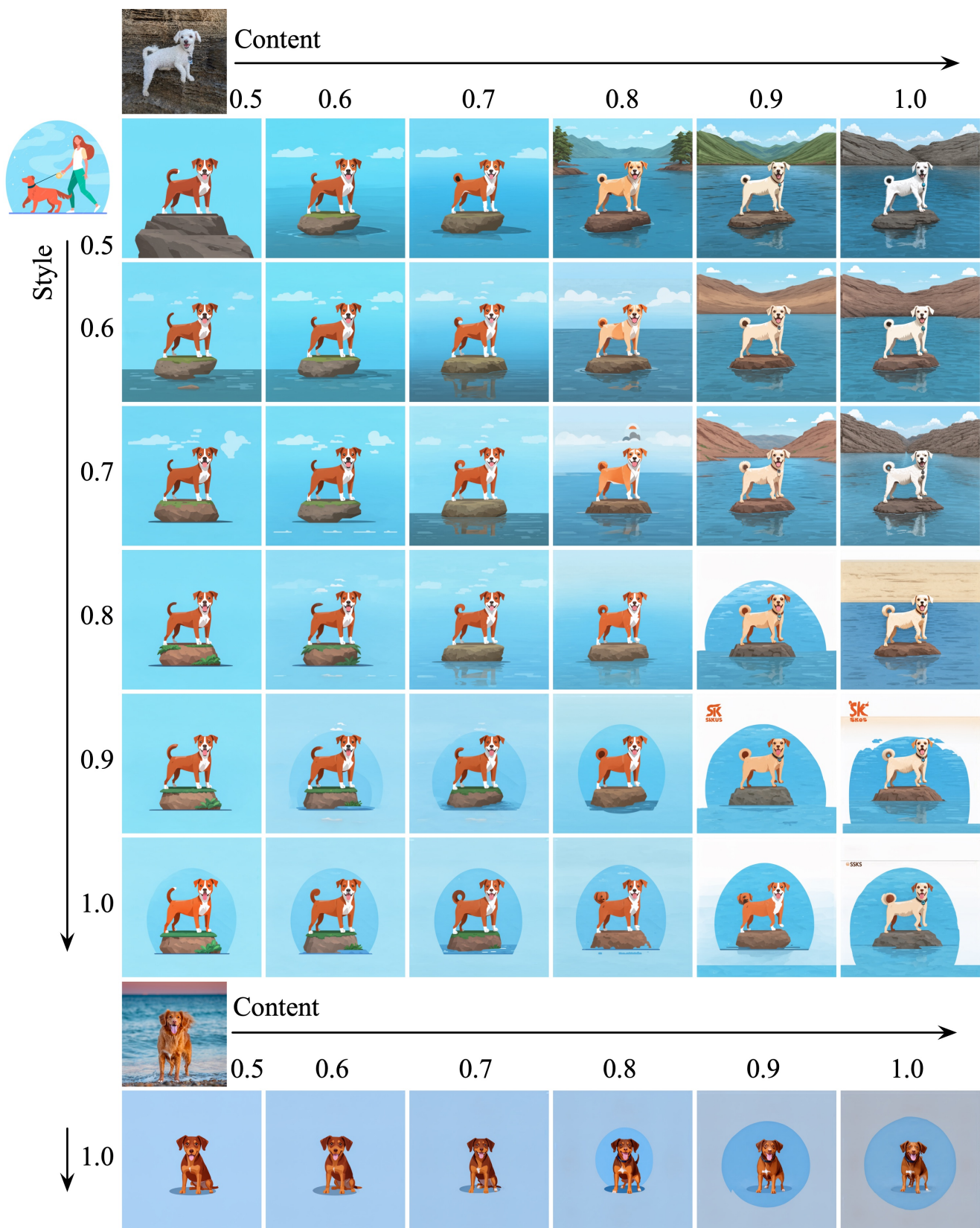


Figure 18. **Comprehensive ablation study on scaling coefficients for content-style fusion based on SD3.** We demonstrate the generation results under various combinations of content and style scaling coefficients. The experiments validate the flexibility and robustness of our approach in achieving fine-grained control over content-style fusion through different coefficient combinations. Please zoom in to view details.

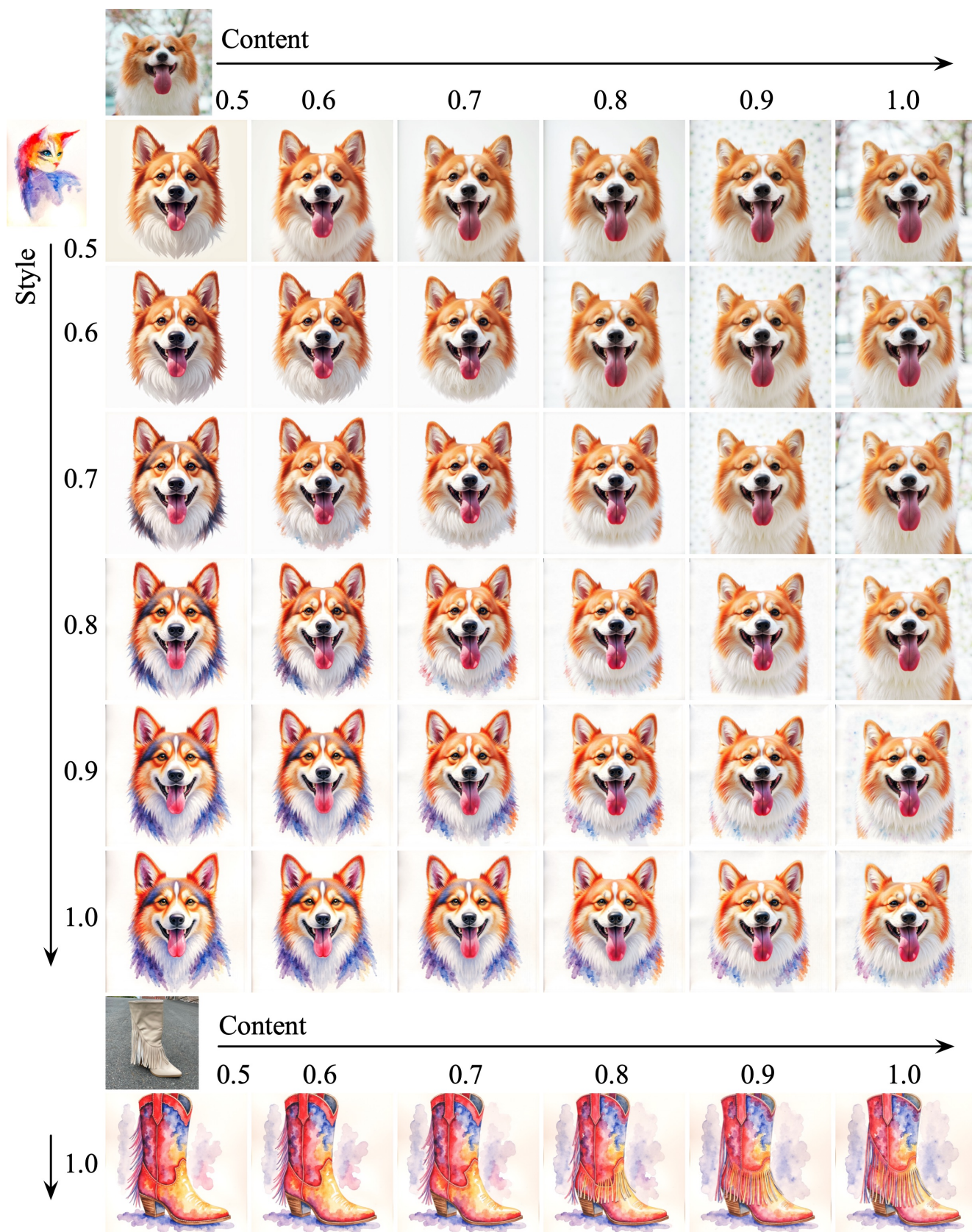


Figure 19. **Comprehensive ablation study on scaling coefficients for content-style fusion based on FLUX.1-dev.** The experiments validate the flexibility and robustness of our approach in achieving fine-grained control over content-style fusion through different coefficient combinations. Please zoom in to view details.

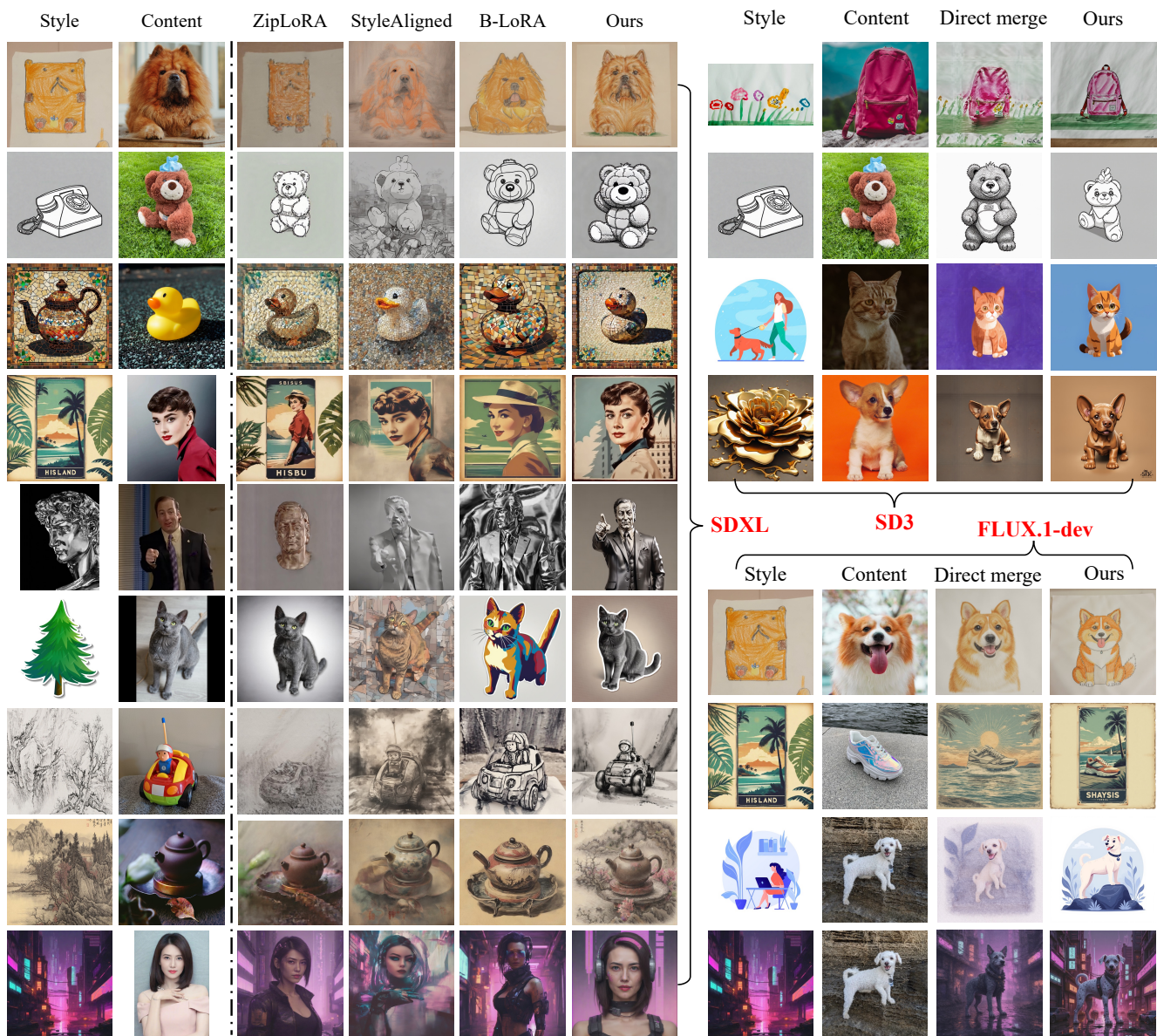


Figure 20. **Extended qualitative comparison results.** Comparison of QR-LoRA against state-of-the-art methods on SDXL, SD3, and FLUX.1-dev models, demonstrating consistent superior performance across different scenarios. Please zoom in to view details.

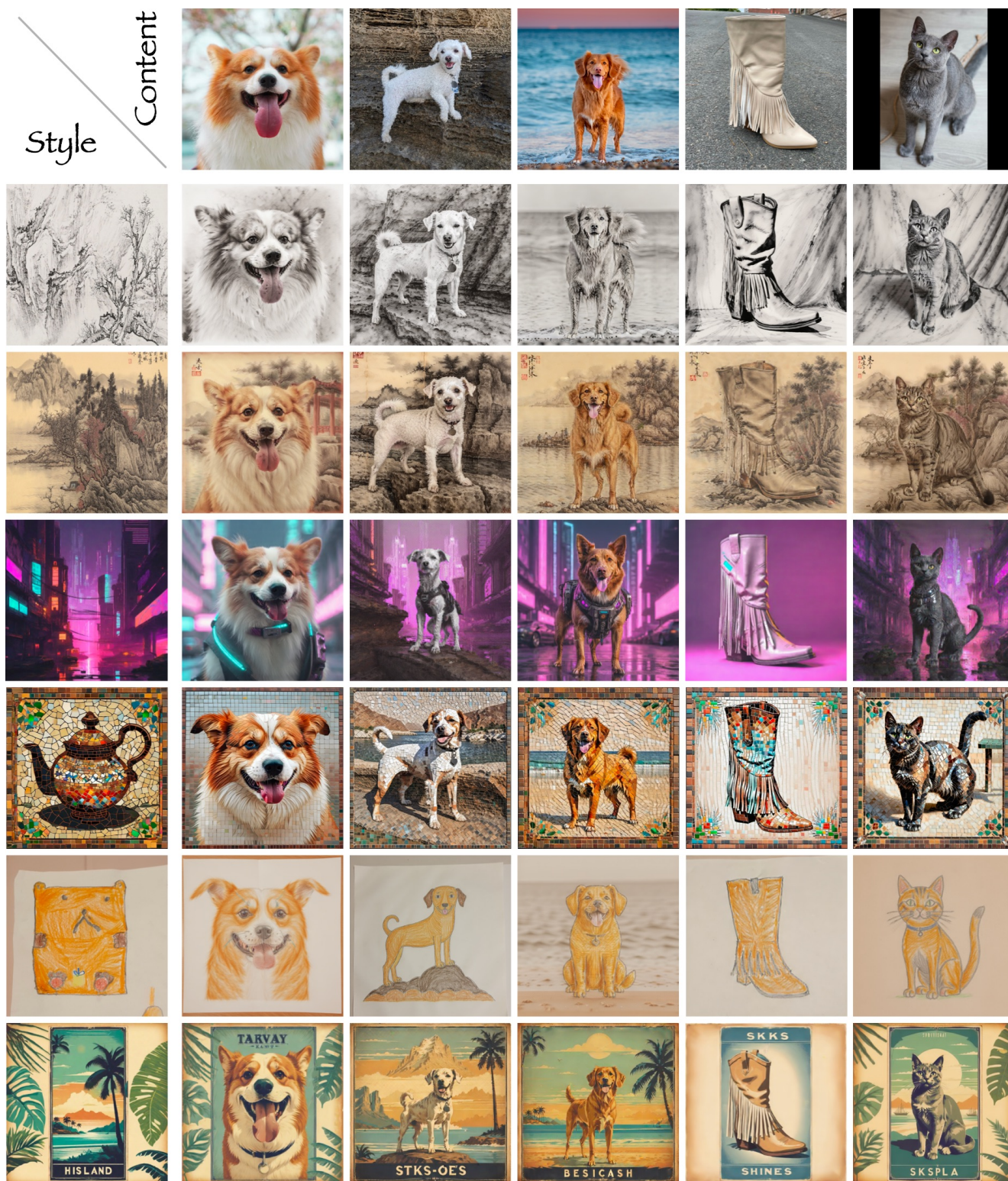


Figure 21. **Diverse generation results based on SDXL.** Additional examples showcasing QR-LoRA’s capability in handling various style-content combinations. Our method successfully preserves intricate content details while effectively transferring diverse artistic styles, from painterly effects to digital art aesthetics. Please zoom in to view details.

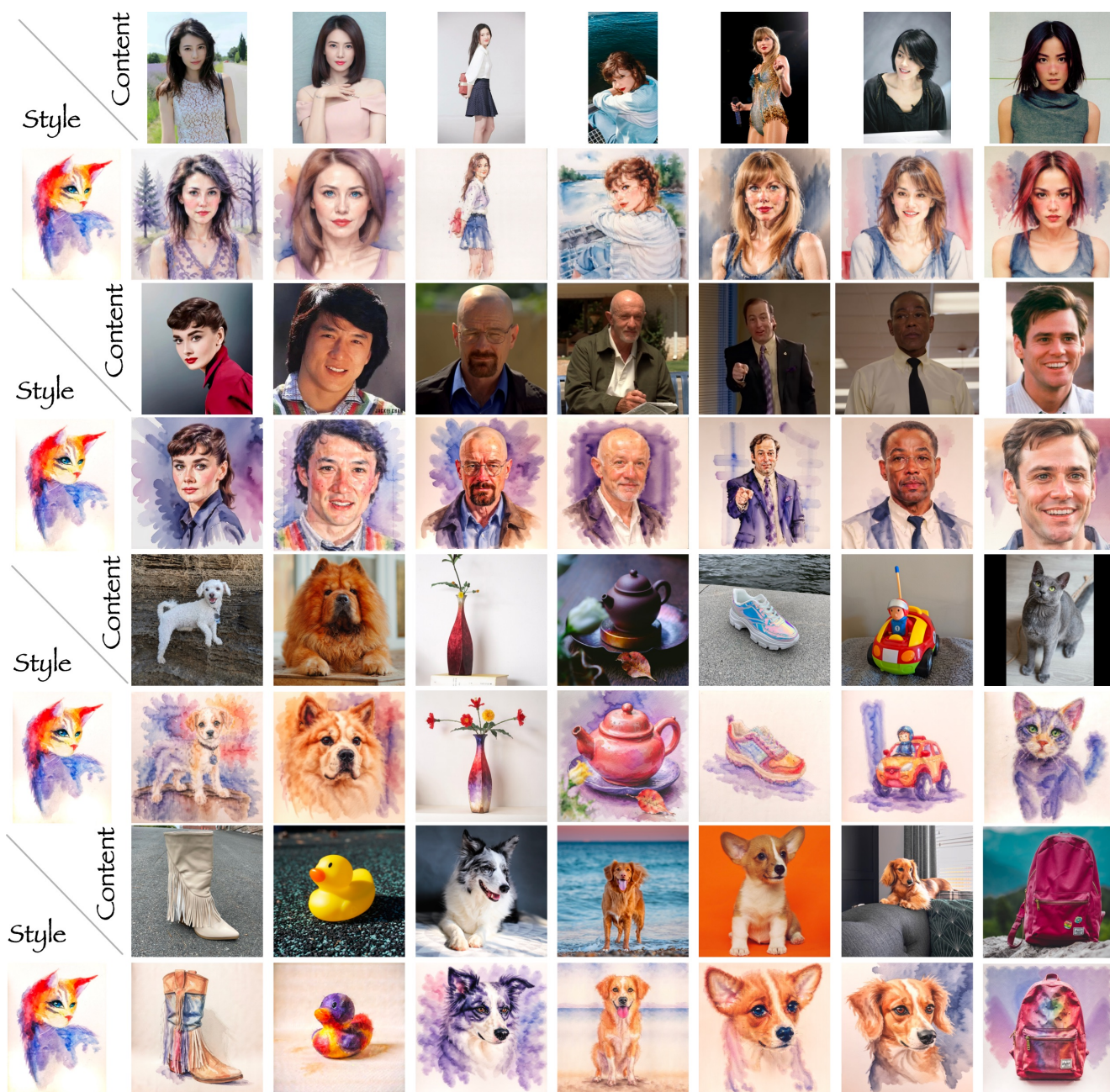


Figure 22. **Diverse generation results on SDXL.** Additional examples showcasing QR-LoRA’s capability in handling various style-content combinations. Our method successfully preserves intricate content details while effectively transferring diverse artistic styles, from painterly effects to digital art aesthetics. Please zoom in to view details.

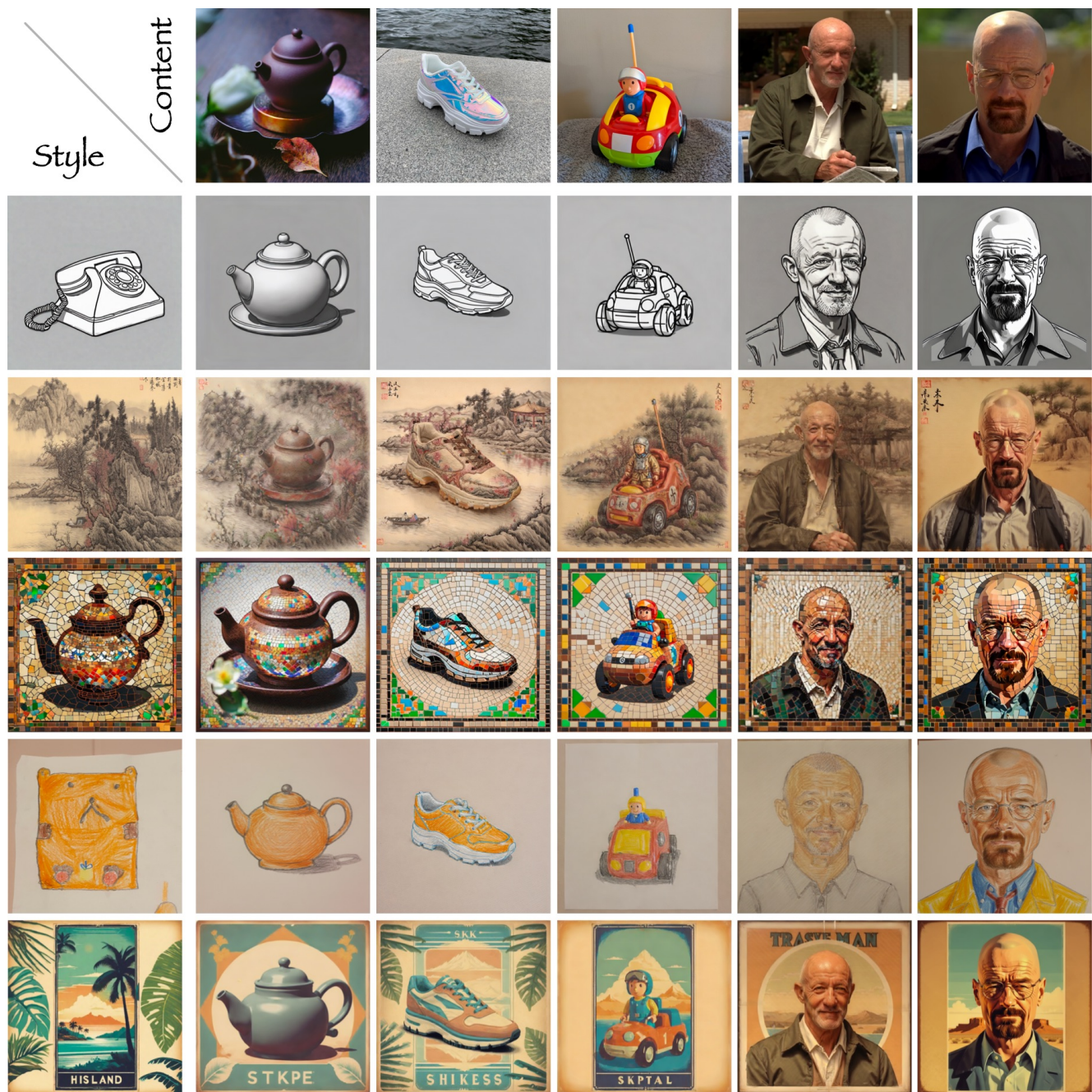


Figure 23. **Diverse generation results on SDXL.** Additional examples showcasing QR-LoRA’s capability in handling various style-content combinations. Our method successfully preserves intricate content details while effectively transferring diverse artistic styles, from painterly effects to digital art aesthetics. Please zoom in to view details.

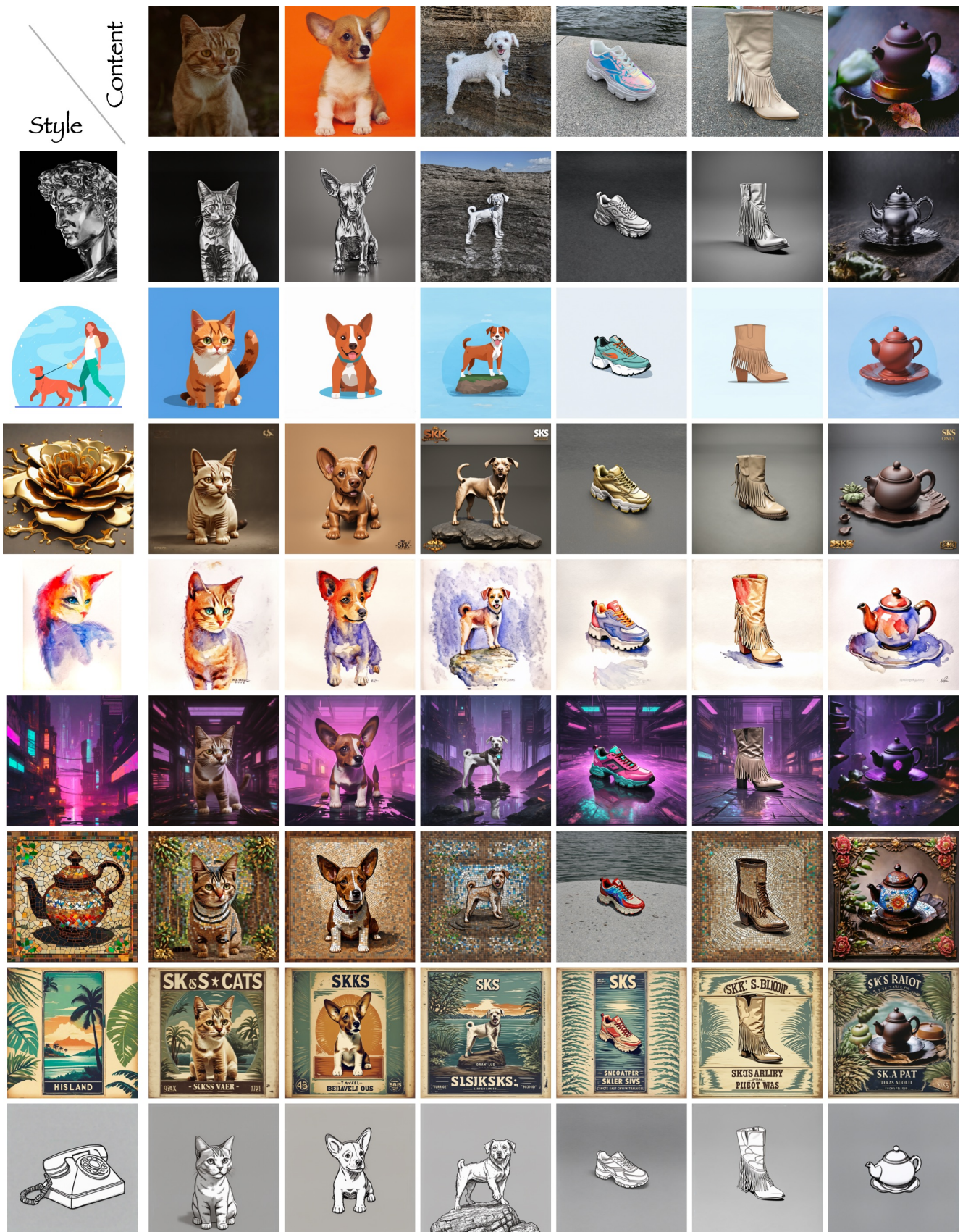


Figure 24. **Diverse generation results on SD3.** Additional examples showcasing QR-LoRA’s capability in handling various style-content combinations.

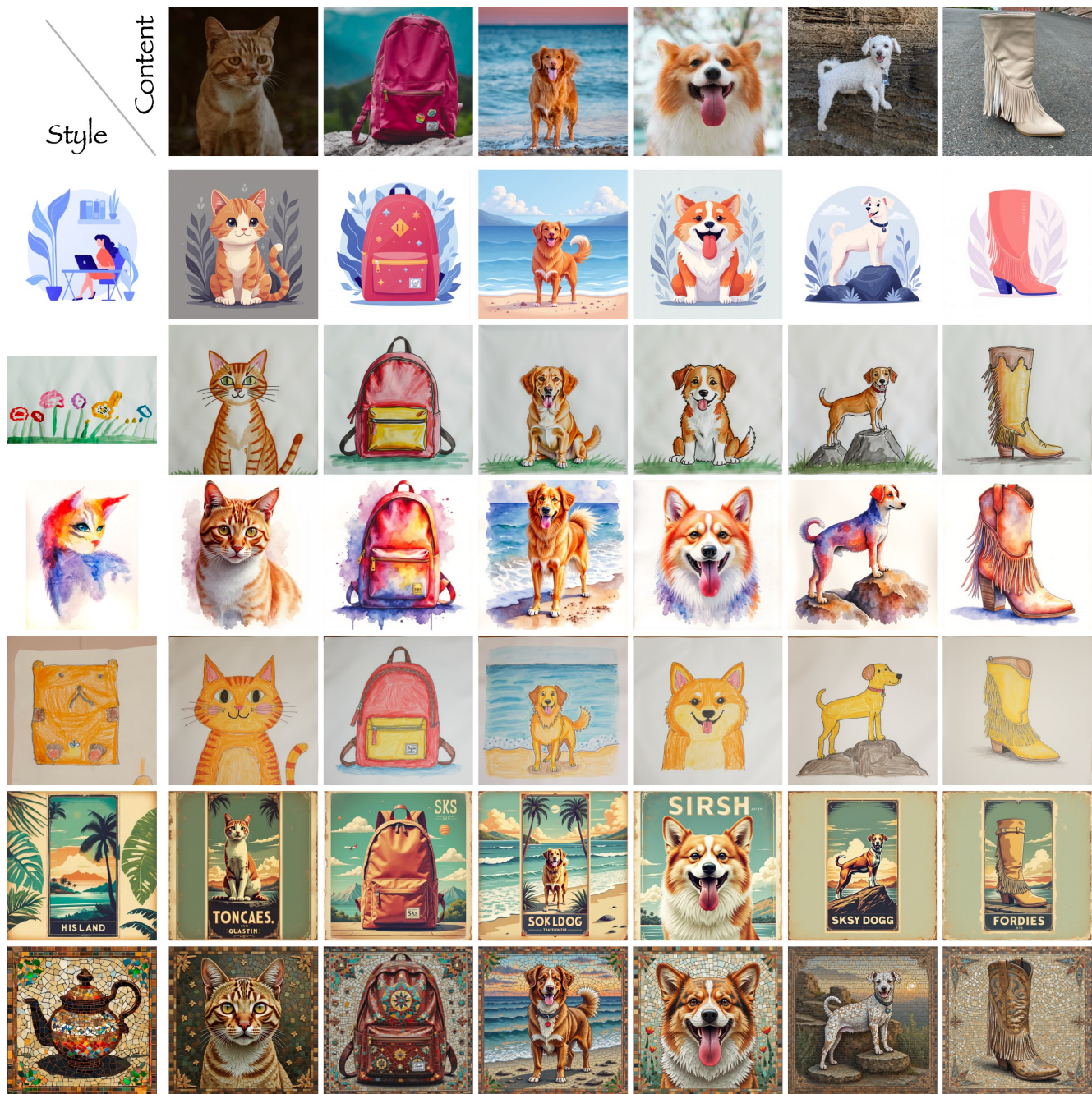


Figure 25. **Diverse generation results on FLUX.1-dev.** Additional examples showcasing QR-LoRA’s capability in handling various style-content combinations. Our method successfully preserves intricate content details while effectively transferring diverse artistic styles, from painterly effects to digital art aesthetics. Please zoom in to view details.

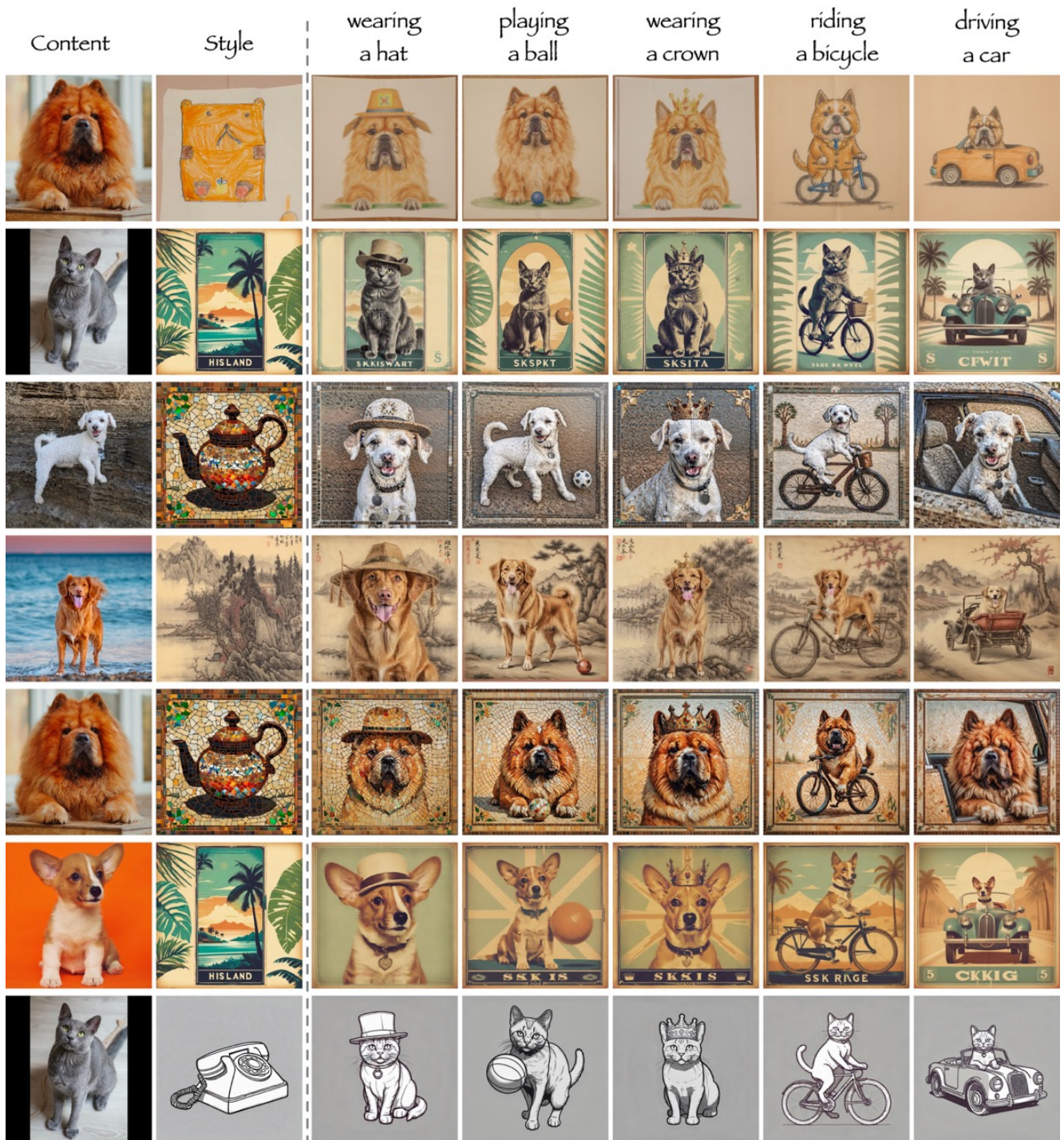


Figure 26. Demonstration of our method’s re-contextualization capability. Given a content image and a style reference, our approach can generate variations through additional text prompts while maintaining style consistency. The examples show how different textual instructions (*e.g.*, “wearing a hat”, “riding a bicycle”) guide the generation process to create diverse scenarios while preserving the original style characteristics.